PROGRESS REPORT OF RESEARCH

on

"THEORETICAL AND EXPERIMENTAL STUDIES OF MAGNETO-AERODYNAMIC DRAG AND SHOCK STAND-OFF DISTANCE"

Contract No. NsG547

for the period

July 8, 1965 through January 7, 1966

GAS DYNAMICS LABORATORY
Department of Mechanical Engineering
and
Astronautical Sciences
Northwestern University
Evanston, Illinois

RESEARCH INVESTIGATORS

Cheng F. Chang:	Research Assistant
Stanley C. Kranc:	Graduate Student Trainee
Robert J. Nowak:	Graduate Student Trainee
Robert W. Porter:	Research Assistant
M. C. Yuen:	Faculty Investigator and Assistant Professor
Ali Bulent Cambel:	Principal Faculty Investigator and Walter P. Murphy Professor of Mechanical Engineering and Astronautical Sciences

TABLE OF CONTENTS

LIST OF FIGURES

NOMENCLATURE

Re_m	magnetic Reynolds number
ρ	plasma density
M_∞	free stream Mach number
γ	ratio of specific heats
N_e	electron number density
T_e	electron temperature
α	recombination coefficient
A^+	argon ion
A^*	excited argon atom
A	argon atom
e	electron
h	Planck's constant
ν	frequency
σ	plasma conductivity
$\overline{V}$	flow velocity
$\overline{B}$	magnetic induction vector
D_a	aerodynamic drag
C_D	drag coefficient
q_∞	free stream dynamic pressure
d	diameter of body
S	magnetic interaction parameter

R_b	radius of body
P_∞	free stream pressure
B_o	magnetic field at stagnation point
V_∞	free stream velocity
T_∞	free stream temperature
Re	Reynolds number
ϵ	density ratio across shock $= \frac{\rho_\infty}{\rho_s}$
r_o	center of magnetic dipole
$\dot{m}$	mass flow rate

INTRODUCTION

In this progress report are summarized the findings of experimental and analytical research concerning NASA Contract No. NsG547 entitled "Theoretical and Experimental Studies of Magneto-aerodynamic Drag and Shock Stand-off Distance." This report covers the period July 8, 1965 through January 7, 1966.

In the progress report covering the preceeding six months period a critical survey of the existing literature was completed and a variety of design calculations comparing "in flight" with "laboratory" data were presented.

It is evident from the literature survey that almost all existing analyses assume that either the magnetic Reynolds number tends to infinity $Re_m \to \infty$ or that the plasma density is constant $\rho = c$. Although neither of these assumptions is realistic it appears that the latter is more plausible. However, this anticipation remains to be justified and it is the objective of the present study to do so.

The present progress report addresses itself to the following aspects of the research program:

1) THEORETICAL CONSIDERATIONS
    - 1.1) Plasma diagnostics
    - 1.2) Magnetogasdynamic drag
2) EXPERIMENTAL STUDIES
    - 2.1) Electromagnet performance
    - 2.2) Plasma diagnostic measurements

2.3) Effect of magnetic field on the flow field and shock stand-off

2.4) Magnetogasdynamic drag

2.5) Magnetogasdynamic heat transfer

3) CONCLUSIONS

1. THEORETICAL CONSIDERATIONS

The analytical studies performed since the previous progress report deal with plasma diagnostics and the magnetogasdynamic drag.

1.1) Plasma Diagnostics

A digital computer program has been employed to obtain tables of data concerning supersonic flow about wedge pressure and total pressure probes. The flow is assumed to be chemically frozen. Preliminary charts for wedge probes of 10, 15 and 20 degree half angle have been prepared. Entry into the charts with experimentally determined wedge pressure and total pressure ratios allows determination of the Mach number and specific heat ratio. The charts of the programs further allows determination of these quantities through measurement of the wedge pressure of two probes of different half angle.

A second digital computer program has been developed. This program converts the measured radiation intensity distribution from an axisymmetric plasma jet into a radial intensity distribution. The novelty of the program is:

a. It does not numerically calculate derivatives and is, therefore, accurate in the presence of shock waves;

b. It avoids slow access storage space and can divide the jet into a greater number of zones than before.

The program is used for diagnostics of photographs of flow about bodies with and without magnetic field after the photographs have been analyzed by the GDL iso-densitometer. It is also used in spectroscopic diagnostics.

12.) Magnetogasdynamic Drag

Some simple theoretical predictions of percentage increase in drag have been compared with GDL experimental data. The flow was nominally Mach 2.75 at .0005 atmospheres with two stagnation temperatures estimated at 7600°K (Run 1) and 10,900°K (Run 2) respectively. Argon was used. Figure 1.2.1 was used to estimate the magnetic interaction parameter. This figure was based on equilibrium flow and is an updated version of that of Reference 1. The engineering estimates of Reference 1 are compared with experiment in Figure 1.2.2. Also shown (dashed curves) are results of a consistant linearized theory based on constant property viscous flow. Both theories assume that the flow and magnetic field are undisturbed and apply only for low magnetic interaction parameter. Since the effect of high interaction is to distort the flow and flux fields in such a way as to tend to reduce the driving effect, the theory would be expected to be high compared with the actual case. This is the case in Figure 1.2.2 but part of the discrepancy may be in non-equilibrium effects. A more exact theory, now in progress, should help to define the situation and evaluate experimental results and existing theory.

The evaluation of existing theories is continuing. A discre-

pancy between shock stand-off distance predicted by Reference 2 and Reference 3, is described in Reference 4 by the present investigators. Essentially, Reference 1 predicts a much larger increase in stand-off then the earlier work of Bush (Ref. 2). Reference 1 employed a more elaborate computational scheme and this scheme was employed by the present investigators. Results are shown in Figure 1.2.3. Unfortunately, the method fails to converge to the correct solution at large magnetic parameter (as was the case in Reference 1). Our computation reduces the discrepancy, but is not yet conclusive since the full range of parameters have not yet been duplicated.

Our calculation of Figure 1.2.3 employs the quasilinerization algorithm to obtain the solution to the non-linear, two point boundary value problem that describes the constant property flow behind the bow shock in high speed magnetogasdynamic flow (the technique of Reference 1). Other algorithms are currently being explored. These include "back and forth integration" and the application of an extremal condition for obtaining a solution. It is believed that these techniques will allow a solution over a much wider range of parameters and allow better evaluation of experiment and theory.

2. EXPERIMENTAL STUDIES

The underlying objectives of the experimental studies performed during this period were to: (a) calibrate the electromagnet performance; (b) determine some of the plasma properties and (c) to obtain a qualitative and quantitative understanding of the interaction between the plasma flow field and the magnetic field.

2.1) Electromagnet Performance

The electromagnet incorporated into the model is a solenoidal magnet wound on a soft iron core. A variety of magnets were designed and tried out. Typical characteristics of these magnets are approximately as follows: wire - 19 gauge anaconda HML copper wire; core - 3/8" diameter Armco ingot iron; coil resistance - 1.8 Ohms; approximate outside dimensions - 1 1/2" long x 2 1/2" diameter, (round nose). In the current series of tests magnetic field strengths up to 7 kilo-gauss were used.

Two types of power supplies have been used, a commercial power supply and a battery supply. The specifications are as follows: Commercial supply - Davenport Model VD 2-30K-1E; DC power supply - 30 amp, 200 volts. Battery supply - Volta commercial grade storage cells rated at 60 ampere hours. The commercial supply provides continuous current for magnetic fields less than 4000 gauss. The batteries are used in 4 banks of 8 cells, each bank providing 100 volts. These banks may then be connected in series or parallel arrangements to provide currents to 200 amps for short times at various voltages. The commercial supply is then used to recharge the batteries thus providing a versatile supply for a wide variety of experiments. In Figure 2.1.1 is shown the performance characteristic of the commercial power supply and in Figure 2.1.2 the performance with the battery power supply. Our experience indicates that we will be able to increase the magnetic field strength further.

Tests were conducted to determine the configuration of the magnetic field distribution both on and off axis. To determine the general shape of the field lines a point mapping of the lines of force was

accomplished by using a small (1/2") compass needle. These results and the field lines of a true dipole at the center of curvature of the body are shown in Figure 2.1.3. Here the solid lines represent the actual field mapping and the dashed lines represent a dipole superimposed on this mapping for comparison. Probe measurements along the axis to determine the drop-off of field with distance are compared to a theoretical dipole in Figure 2.1.4. The disagreement between experimental and theoretical results is not severe, especially in the region of interaction.

2.2) Plasma Diagnostic Measurements

For purposes of determining the free stream Mach number, M_∞ and the ratio of specific heats, γ, it is assumed that the plasma is a chemically frozen perfect gas. Hence, the specific heat and molecular weight are assumed constant.

We have employed two methods for determining M_∞ and γ. The first consists of traversing, in a normal direction, the plasma stream with a blunted 15° cone which measures the stagnation impact pressure. Also, the plasma is tranversed with a single wedge probe which measures the wedge pressure. (See Figure 2.2.1 for a typical survey). Then a digital computer program is used to determine M_∞ and γ. The program generates M_∞, stagnation pressure ratio, and wedge pressure ratio from inputs of wedge half angle, Mach angle, and γ for a given wedge-half-angle. The required data are, stagnation pressure ratio, wedge pressure ratio, and wedge-half-angle.

The second method consists of surveying the plasma stream with three wedges of half angles 10^{o}, 15^{o}, 20^{o}. Then utilizing the aforementioned computer program and two wedge angles and the two corresponding wedge pressure ratios, M_{∞} and γ are determined. The second method using the data from the 10^{o} and 15^{o} wedges has proved to be more satisfactory. It is believed that the 20^{o} wedge and the stagnation pressure probe disturb the flow to an extent that γ is not constant across the respective shocks.

Some difficulty has been encountered in accurately measuring the wedge pressure for wedge half angles of 10^{o} and less. But efforts are being made to resolve the problem.

The results of this part of the diagnostic work indicates that γ is between 1.1 and 1.2 and that M_{∞} is about 2.75 under present operating conditions.

2.3) <u>The Effect of the Magnetic Field on the Flow Field Around the Body</u>

Ordinarily the data in such work are interpreted visually and manually. However, this leads to inconsistencies and to crude readings. Accordingly, we obtained a microdensity tracer which is able to perform the following operations:

a. Plot film density as a function of lateral position for a single line across a film negative (or positive print).

b. Automate this operation providing successive scans at small intervals perpendicular to the scan direction.

c. Present this density information for a magnified area of interest from the negative in the form of contours of equal film density.

The experimental set-up consists of the hyperthermal arc jet facility shown in Figure 2.3.1. A hemispherical model containing an electromagnet is introduced into the supersonic plasma stream. Observations are made with and without the magnetic field. In Figures 2.3.2 and 2.3.3 may be seen photographs of the plasma flow about the 3" hemispherical model. In Figure 2.3.2 the electromagnet is inactive whereas in Figure 2.3.3 it is operative. It is clearly evident that the flow configurations are quite different. For example, the intense luminous regime ahead of the body is thickened and enlarged. Second, the configuration of the upstream jet becomes more diffuse. Third, the dark regime ahead of the intense luminous zone in Figure 2.3.2 becomes more diffuse in Figure 2.3.3 although it still exists qualitatively. This dark regime ahead of the intense luminous regime has been considered by Talbot and Grewal (Reference 5) who suggested that it is due to a rise in the electron temperature. They indicate that the dominant recombination reaction is

$$A^+ + 2e \rightarrow A^* + e$$

followed by

$$A^* \rightarrow A + h\nu$$

The recombination coefficient α is

$$\alpha \approx 5.6 \times 10^{-27} (T_e)^{-9/2} N_e$$

Thus a rise in the electron temperature would decrease α and, therefore, the radiation.

The displacement of the luminous region by the magnetic field has been interpreted previously as a thickening of the shock layer.

Careful study of Figure 2.3.3 indicates, however, that the change in brightness extends farther out than what appears to be the shock front. This is especially prominent in the region away from the center line of the body. This may be explained by the fact that the $\sigma(\bar{V} \times \bar{B}) \times \bar{B}$ force can slow down the electrons in front of the shock except those along the center line, and as a result the electron number density N_e increases locally. Since α is proportional to N_e, an increase in N_e would mean more radiation and, therefore, brightness.

In Figure 2.3.4 may be seen a typical isodensity trace of Figure 2.3.2. The position of the model has been drawn in. The flow configuration is clearly symmetric. In this trace the sequence blank-dot-dash means increasing optical density and the sequence dash-dot-blank means decreasing optical density. If we compare the 150 density trace in Figure 2.3.4 with that in Figure 2.3.5 (for the photograph in Figure 2.3.3) we find that the flow field ahead of the model nose is distorted taking on a steeper configuration. Also, the darkened regime ahead of the luminous tract is lengthened. Finally, the uniform flow upstream is affected farther upstream than in the non-magnetic case. These indicate that the color change which we mentioned in our previous progress report may have fluidmechanic implications.

Figure 2.3.6 shows typical film density traces along the center line of the body for different magnetic field strengths. The traces all show a substantial rise in density near the body and a minimum which corresponds to the dark space in front of the shock. Then there is a gradual rise far away from the body indicating a return to the free stream condition.

The shock stand-off distances are determined by two different methods. One is to draw a line of constant density corresponding to the free stream density until it intersects the density trace near the body. The distance between the body and the point of intersection is called the shock stand-off distance. The other method is to take note of the fact that the density traces decrease almost as straight lines near the body. The distance between the point of intersection of this straight line and the line of constant density corresponding to the minimum density and the body is called the shock stand-off distance. The absolute values of the shock stand-off distances by the two methods are different but they give approximately the same percentage increase in shock stand-off. A typical curve of the percentage increase in shock stand-off distance as a function of the magnetic field is shown in Figure 2.3.7. Although there is some scattering in the data, a straight line can be drawn through the data without too much trouble.

It was found that the percentage increase in shock stand-off distance under the same condition is much larger than that of the increase in drag. One plausible explanation is that in the present experimental condition, the friction drag is not negligible. This was predicted in the theoretical analysis in Reference 1. The effect of magnetic field is to reduce the velocity and, therefore, the friction drag. Thus, in the case of drag measurement, the effect of the magnetic field is to increase the Lorentz force and the pressure, but decrease the viscous drag. Hence, the compensating effect makes the total increase in drag small. On the other hand, the increase in shock stand-off distance is simply a consequence of the conservation of mass which does not depend on the vel-

ocity profile, but only on the velocity. Another plausible explanation is that the shock stand-off distance is determined by a measurement of the intensity of radiation. Since the magnetic field can change the luminosity in front of the shock, the present method of measurement may overestimate the change in shock stand-off distance due to the magnetic field.

The usual definition of the shock front is a sharp increase in the particle number density. From spectroscopic work we can find the number density as a function of distance. This will enable us to have a direct check on the above measurement. Meanwhile, further work will be done on the densitometric analysis of the negatives. Particularly we would like to find out the actual variation in density along the center line of the body by the use of Abel inversion.

The problem that appears to be of paramount interest is a categoric understanding and delineation of what the shock front actually is. We are now in the process of undertaking the appropriate measurements. These are as follows:

a. For a quantitative measurement of the electron density N_e and the electron temperature T_e we shall measure the Stark broadening of the H_β(4861 Å) line. For this purpose we have borrowed a Hilger Model E383 F/20 prism spectrograph and constructed a high resolution optical system. This system will also facilitate investigation of the entire optical spectrum at all positions in the flow field. (A similar experiment has been carried out

by Chen (Reference 6) for the case when there is no applied magnetic field). It should be noted that the effect of the magnetic field on line broadening (Zeeman effect) is negligible in comparison with the Stark broadening for a magnetic field below 10 KG. This method should enable us to determine quantitatively the effect of magnetic field on N_e and T_e.

Another problem that we intend to investigate more thoroughly is the change in color ahead of the shock when a magnetic field is present. A preliminary experiment with a spectrograph has shown that in general the effect of a magnetic field is to increase the intensity of a given line although exceptions to this have been observed. Figure 2.3.8 shows the general increase intensity for two typical argon lines. Line B, for example, is approximately 1.3 times more intense with a magnetic field (2) than without (1) at the maximum intensity.

Figure 2.3.9 shows the decrease in intensity as a function of axial position, the least intense profile corresponding to the position farthest from the body. Although this set of profiles was taken with no magnetic field, the effect of increasing intensity with magnetic field has been observed to be a general effect at all axial positions. Line widths appear to be altered with axial position and with magnetic field.

The result of a change in intensity and line width with magnetic field would indicate a change in N_e,T_e and thus α, the recombination coefficient mentioned earlier. It is expected that much more conclusive results will be obtained from new experimental apparatus now being

tested and a complete Abel inversion of the data.

2.4) Drag Measurements

The drag measurement system currently being used is shown in Figure 2.4.1. The electrical output is derived from a commercial force transducer of the linear differential transformer type. Calibration experiments have shown the system to be extremely accurate and linear to about 200 grams. Time response is approximately 1 1/2 seconds. The calibration curves are shown in Figures 2.4.2 and 2.4.3.

Considerable effort has been expended to eliminate mechanical and aerodynamic fluctuations in order that the electrical output may be read accurately. This is accomplished by electronic filtering, a surge tank in the water supply line and a mechanical padding and suspension system.

Using the system described, a number of drag tests were conducted under a variety of flow conditions. The best axial position with respect to aerodynamic fluctuations was found to be at 12 1/2" from the nozzle exit. The tests discussed here were conducted at that position.

It is seen from Figure 2.4.4 that the effect of increasing gas flow to the torch is to decrease the percent alteration in total drag. This is to be expected since the enthalpy of the flow and thus the electrical conductivity decreases and the aerodynamic drag increases.

Figure 2.4.5 shows a number of separate features. The effect of increasing power and thus enthalpy is shown by comparing runs 1 and 2. The effect of increasing the ambient tank pressure is seen by comparing runs 2 and 3. There is no significant change in this case when

the pressure is altered by a factor of nearly 2. For all three runs the effect of increasing magnetic field is shown. Run 2 was the most thoroughly investigated and the solid line is a least-squares linear curve fit to the data. This curve will be extended and runs at higher torch powers are planned.

In addition, a body of ~ 1/2" diameter and the associated magnet have been constructed. The magnet has been tested and is capable of producing a field of about 6000 gauss. The effects of reducing the body sizes are:

a. Reduce the aerodynamic drag

b. Because of the non-uniform flow condition a smaller body would tend to reduce the effect of non-uniformity especially in the electrical conductivity.

Although the increase in drag due to the magnetic field is smaller than the theoretical results, the aerodynamic drag without the magnetic field between theory and experiment indicate good agreement. The calculations are based on the equation

$$D_a = q_\infty \frac{\pi d^2}{4} C_D$$

where q_∞ is the free stream dynamic pressure and C_D is the drag coefficient. In this calculation we use $M_\infty = 2.75$ and $\gamma = 1.1$. C_D is taken to be 1.44 based on previous estimates of pressure, friction and base drag coefficient (from Reference 1). The results of the estimated drag is between 117 gm to 124 gm as compared with the measured value of 112.5 gm. This indicates that the method and accuracy of measurement are basically sound. The large discrepancy between theory and

experiment for total drag is probably due to the simplifying assumptions involved in the calculation.

2.5) Magnetogasdynamic Heat Transfer

An experimental program has been initiated to determine the effect of a magnetic field on the total heat transfer from a supersonic plasma stream to a blunt body. The purpose of the heat transfer work is to provide an experimental check on the theory which predict a reduction in stagnation magnetogasdynamic heat transfer.

The initial phase of this project consisted of a 3 inch diameter flat faced, thin shell model having a single thermocouple on the inside surface of the body at its centerline. Within the non-water cooled body was an electromagnet coil which produced a dipole-like field about the body centerline. The body was kept at an initial uniform temperature by means of a heat shield which was rapidly opened to expose the model to the plasma once desired operating conditions were reached; the heat shield was then closed to permit the body to cool after a test time of about 3 seconds. The highest magnetic field used was 3000 gauss at the stagnation point.

Assuming one dimensional heat transfer to an insulated body, the total heat transfer is proportional to the time-rate of temperature-rise of the body. The initial tests indicated a scatter in the non-magnetic temperature-time slope of the same magnitude as any changes due to a magnetic field. Part of this scatter is believed to be due to the fact that the body never cooled down to the same initial temperature for each test. Thus, it was decided to design and test a

more sophisticated model.

The second heat transfer model consists of a three inch diameter hemispherical thin shell copper body as shown in Figure 2.5.1. The body has thirteen thermocouples located on the inside surface. Within the body is an electro-magnetic coil which produces a dipole-like field about the body centerline. The afterbody has a water cooled base which will cool the body by conduction to the same initial temperature after each test. By monitoring the transient temperature rise of the entire body it will be possible to calculate the heat flux through the body to correct the one dimensional heat transfer assumption. Also, it will be possible to determine the MHD effect on heat transfer at positions on the body other than the stagnation point. The magnetic field has been mapped over the hemispherical portion of the body (see Figures 2.5.2 and 2.5.3). The highest field at the stagnation point is rather low, only about 4400 gauss. The reason for this is that the thermocouples inside the body make it difficult to position the coil as close to the stagnation point as would be desired.

Initial heat transfer measurements with the hemispherical body indicate that the stagnation temperature rise without magnetic field is repeatable for several tests. These tests also indicate that the transient temperature has a gradient over the surface of the body. Thus, a correction to the one dimensional heat transfer assumption may be required. The initial measurement with a magnetic field of 4400 gauss indicates that the field affects the temperature rise of the body. At the stagnation point the rate of temperature increase is

reduced; the effect appears to be more pronounced away from the stagnation point. Consequently, further measurements are being undertaken to obtain a concrete picture of the temperature rate and magnetic field interaction. With more information, it will be possible to establish the reduction of total heat transfer to the body due to a magnetic field. Also, using the diagnostic results, it may be possible to determine the change in the heat transfer coefficient due to the magnetic field.

3. CONCLUSIONS

From the results of our research program we conclude the following:

1) A diagnostic technique has been developed and used to measure M_∞ and γ. This technique involves interpretation of experimental pressure measurements by means of computer-generated tabular data.

2) Magnetogasdynamic drag measurements have been made under a variety of flow conditions and these results are compared with theoretical predictions. It appears that the observed discrepancy is due to simplifying assumptions made in the theoretical predictions.

3) The shock stand-off data presented was measured by a method which depends on the luminosity of the flow. It is found that aside from the predicted increase in shock stand-off the luminosity is altered ahead of the shock.

4) In conjunction with the general program of research, an experiment is in progress to determine the alteration in heat transfer to the body with magnetic field.

REFERENCES

1. "Design Calculations for Magnetoaerodynamic Drag", Gas Dynamics Laboratory, Northwestern University, April, 1965. (Submitted to NASA in conjunction with NsG547.

2. Smith, M. C., Schwimmer, H. S. and C. S. Wu, "Magnetohydrodynamic-Hypersonic Viscous and Inviscid Flow Near the Stagnation Point of a Blunt Body", AIAA J. 3, July, 1965, pp 1365-1367.

3. Bush, W. B., "Magnetohydrodynamic-Hypersonic Flow Past a Blunt Body", J. Aero. Sci., 25, November, 1958, pp 685-690, 728.

4. Porter, R. W. and A. B. Cambel, "Comment on 'Magnetohydrodynamic-Hypersonic Viscous and Inviscid Flow Near the Stagnation Point of a Blunt Body'", (Submitted to the AIAA J., Sept. 1965.)

5. Grewal, M. S. and Talbot, L. "Shock Structure in a Partially Ionized Gas", Journal of Fluid Mechanics, Vol. 8, Part 3, pp 465-480, July 1960.

6. Chen, C. J., "Spectroscopic Measurement of a Detached Shock Wave in an Arc Heated Plasma Jet", Vol. IV, JPL Summary Reports, No. 37-32.

Activities

Publications

Anderson, Thomas P., "Lorentz Drag: An Engineering Approximation", Journal of Spacecraft and Rockets, Vol. 2, No. 5, p. 810, Sept.-Oct. 1965 (with Robert B. Bass).

Cambel, Ali Bulent, "Observations Concerning Magnetoaerodynamic Drag and Shock Stand-off Distance", Scheduled for publication in the March 1966 issue of the Proceedings of the National Academy of Sciences(with G. Seemann).

Cambel, Ali Bulent, "Magnetoaerodynamic Re-entry", Paper 66-161, To be presented at AIAA Plasmadynamics Conference, March 2-4, 1966 Monterey, California (with R. Nowak, S. Kranc, R. Porter, and M. C. Yuen).

Cambel, Ali Bulent, "Comment on Magnetohydrodynamic - Hypersonic and Inviscid Flow Near the Stagnation Point of a Blunt Body", Scheduled for publication in the AIAA Journal (with R. Porter).

Cambel, Ali Bulent, "Plasma Physics", D. C. Heath Co. 1965 (with Marion Cambel) The preface of this book acknowledges the support of NASA to the senior author's research.

Ph.D. Theses in Progress

Porter, Robert: "Analytical Study of Magnetoaerodynamic Shock Stand-off and Drag".

Kranc, Stanley: "Experimental Study of Magnetoaerodynamic Drag and Shock Stand-off Distance".

Chang, C.: "Ifluence of Electric Currents on Magnetoaerodynamic Drag".

Nowak, Robert: "Heat Transfer Effects During Magnetoaerodynamic Re-entry".

Other Activities

Ali Bulent Cambel was awarded the Outstanding Achievement Award of the Immigrants Service League for contributions to science and education. Previous recipient was S. Chandresekhar.

Ali Bulent Cambel was elected a Congress Survey Lecturer for the 5th U. S. National Congress on Applied Mechanics to be held June 1966. Previous invited lecturers on fluid mechanics were Theodore von Kármán,

Richard von Mieses and Howard Emmons. Acknowledgement is made to NASA in this paper.

A paper by Ali Bulent Cambel entitled, "Magnetogasdynamics: Its Science and Technology" was chosen by a national committee including several Nobel Laureates for inclusion in the 5000 year Westinghouse-University of Pennsylvania Time Capsule as being symbolic work of its era.

The Ford Motor Company made an award to Ali Bulent Cambel for "...outstanding contributions to curriculum development".

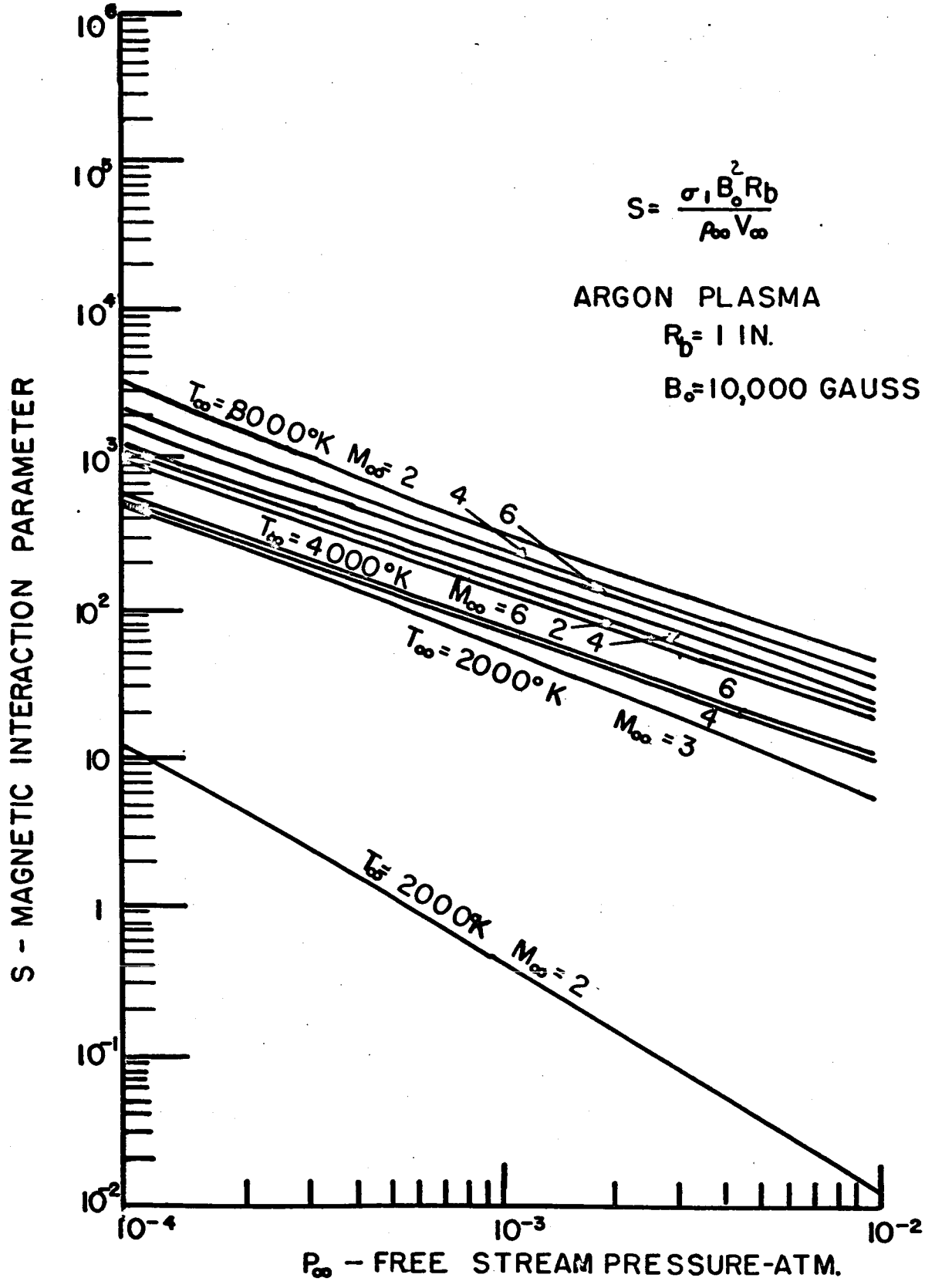

MAGNETIC INTERACTION PARAMETER
REAL GAS FLOW OF ARGON

FIG. 1.2.1

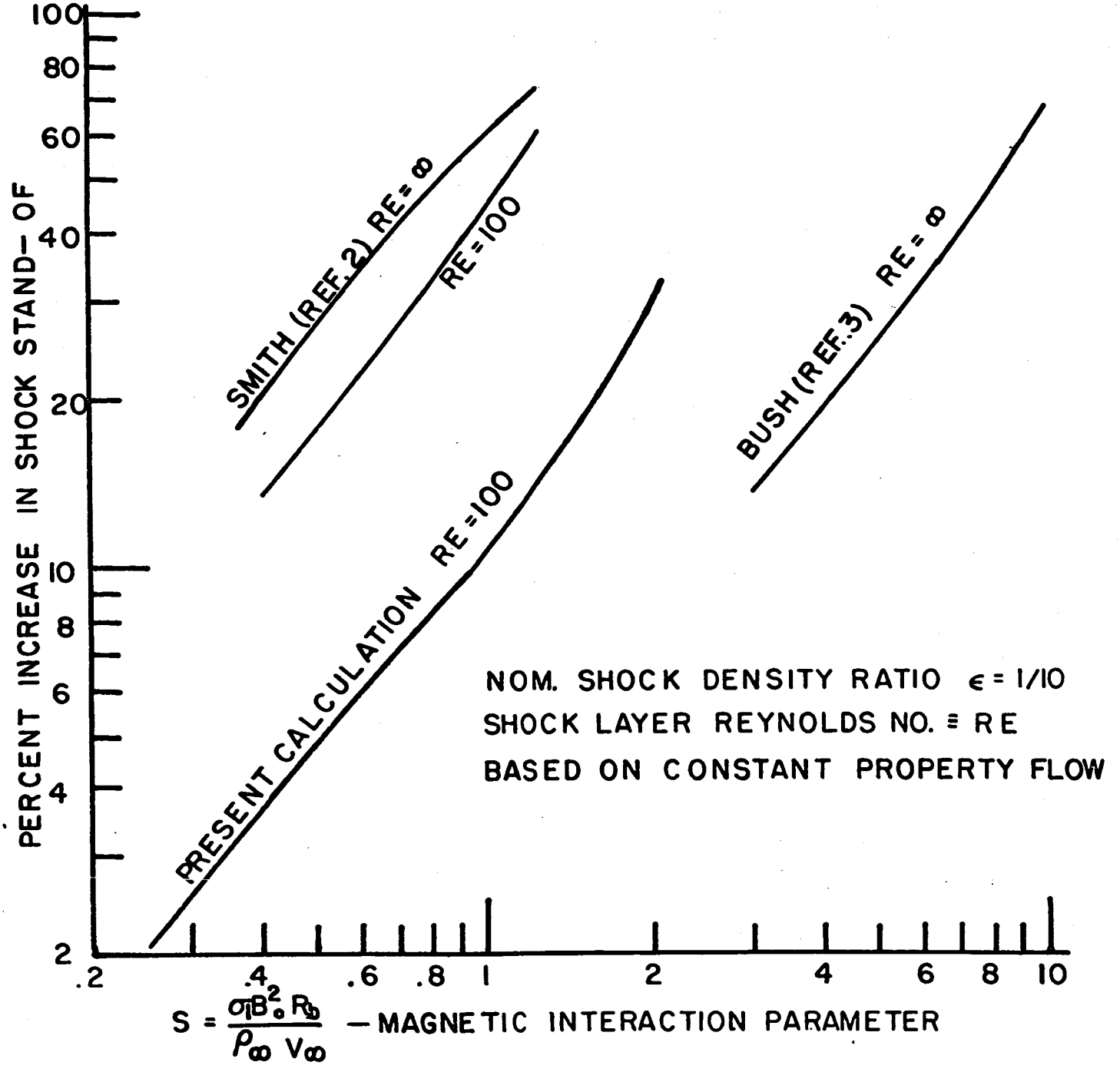

COMPARISON OF THEORIES PREDICTING INCREASE IN SHOCK STAND-OFF DISTANCE

FIG. 1.2.3

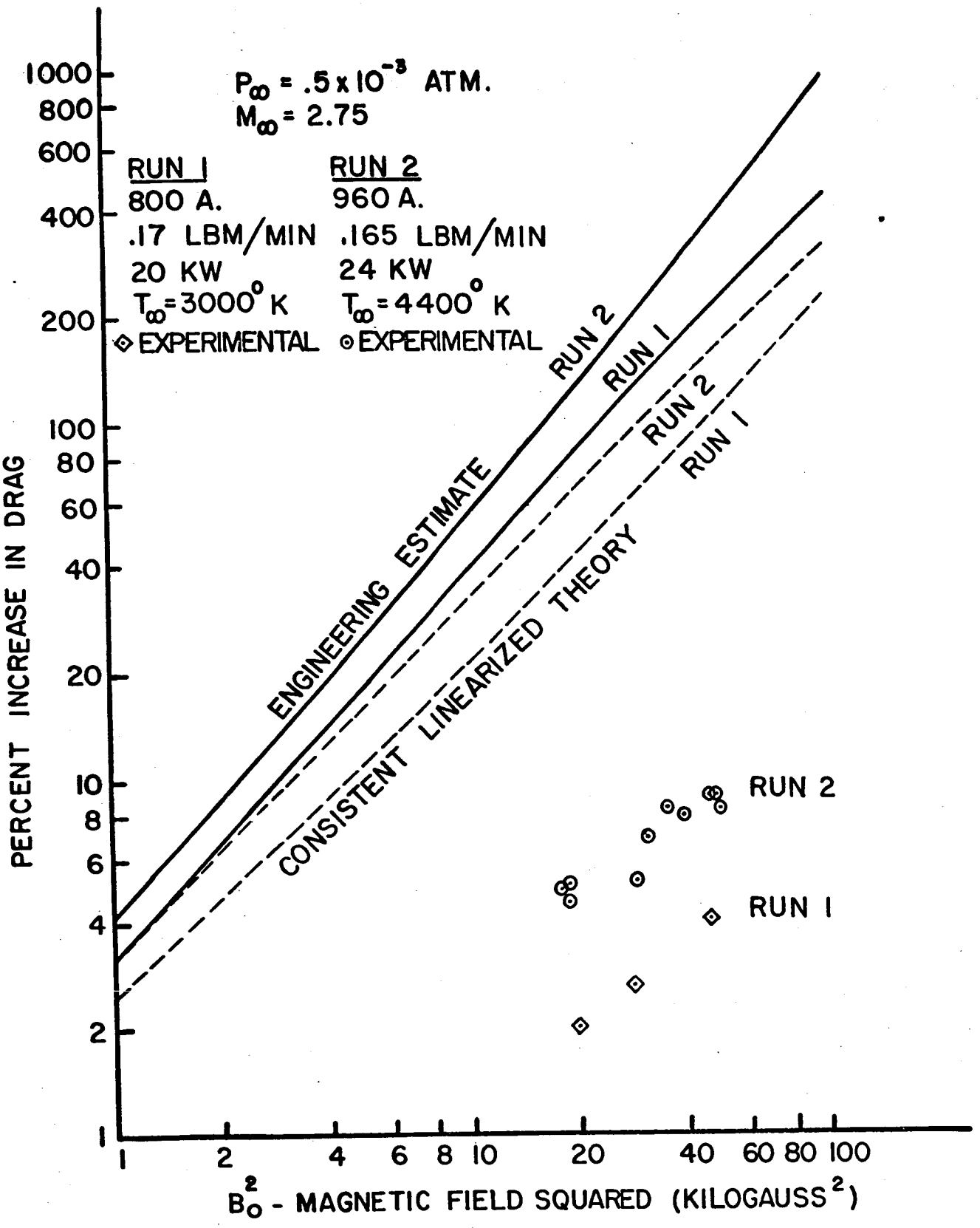

COMPARISON OF GDL EXPERIMENTAL DATA WITH ESTIMATES BASED ON EQUILIBRIUM THEORY & WEAK INTERACTION

FIG. 1.2.2

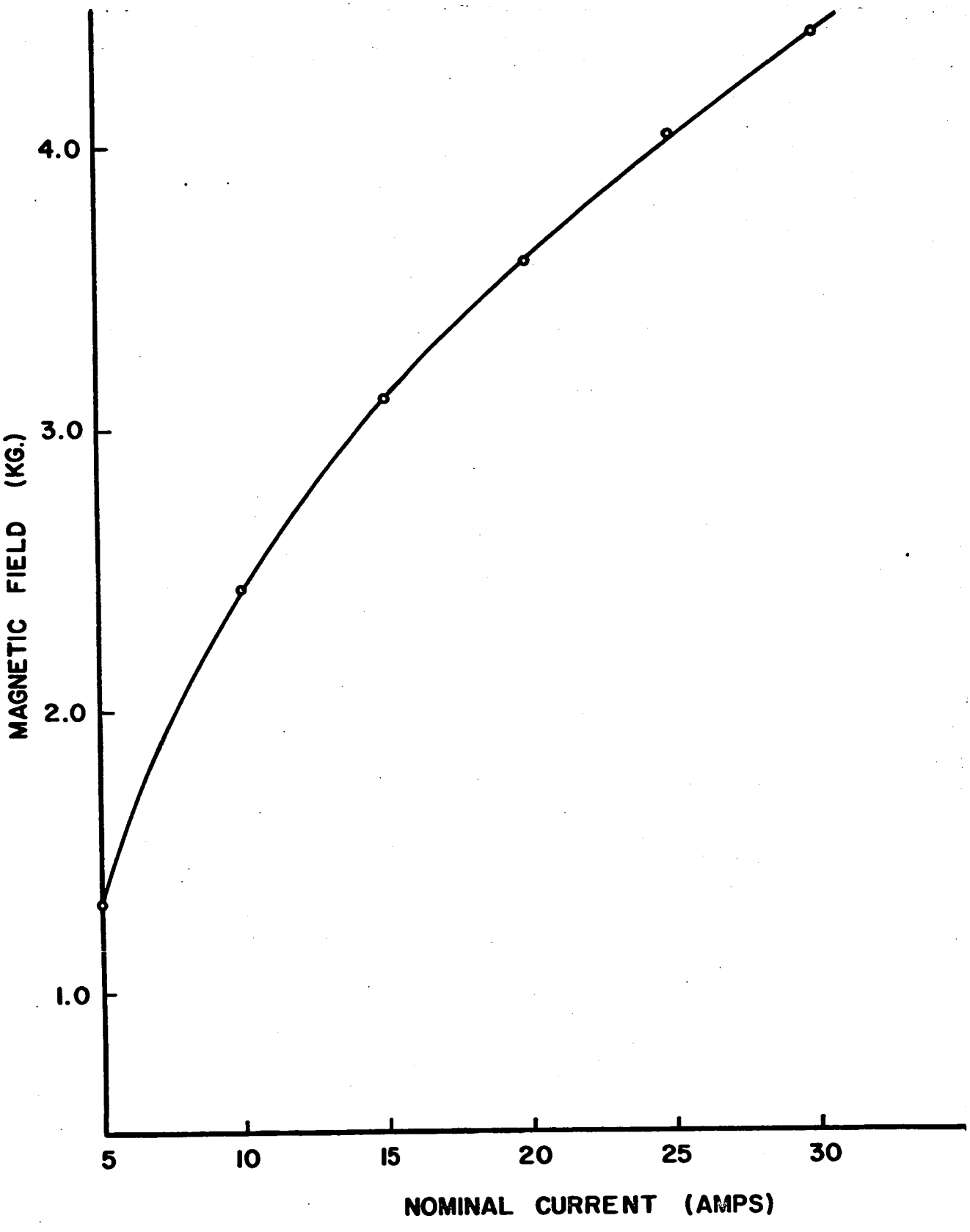

MAGNETIC FIELD STRENGTH AT STAGNATION POINT (COMMERCIAL SUPPLY)

FIG. 2.1.1

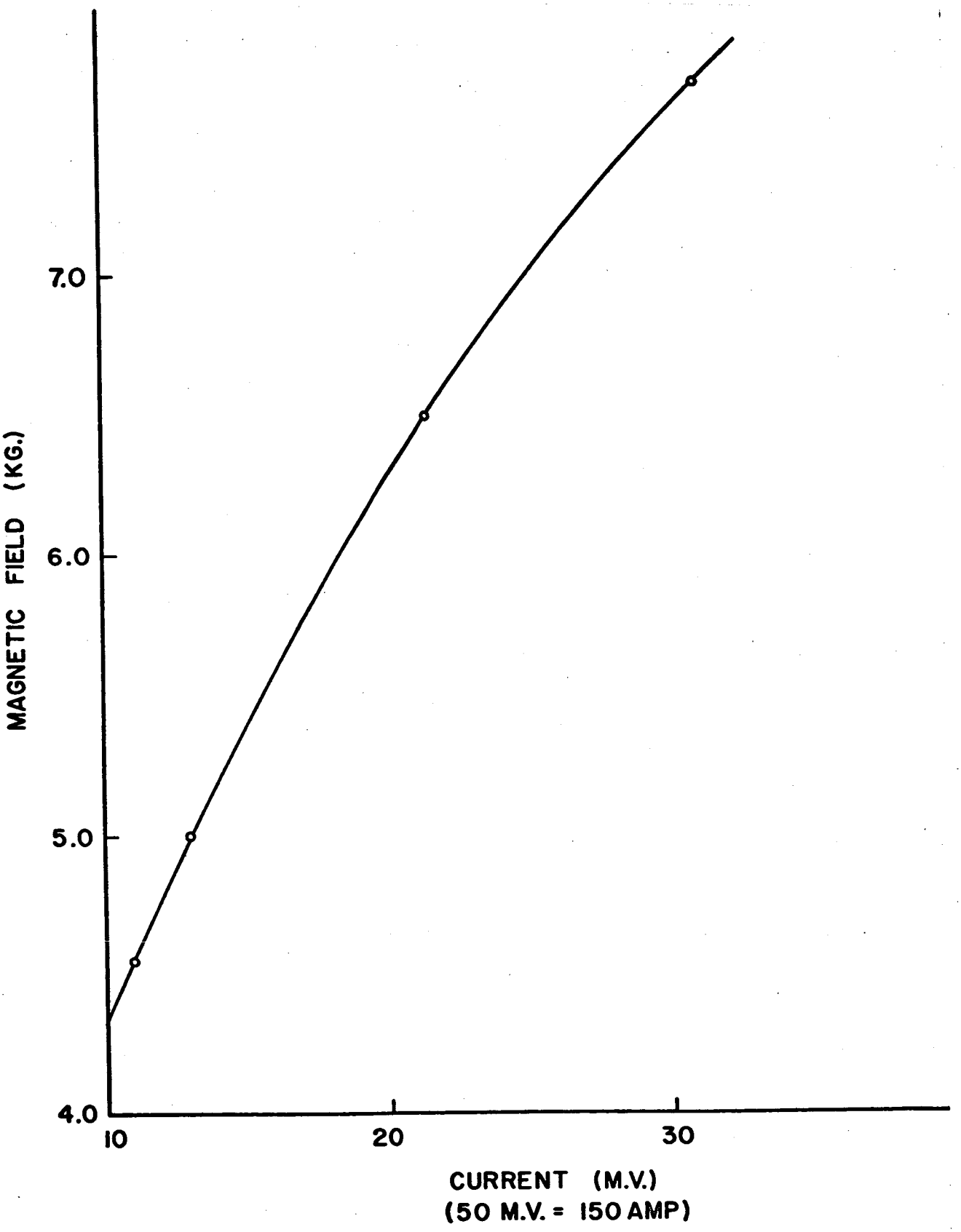

MAGNETIC FIELD STRENGTH AT STAGNATION POINT (BATTERY SUPPLY)

FIG. 2.1.2

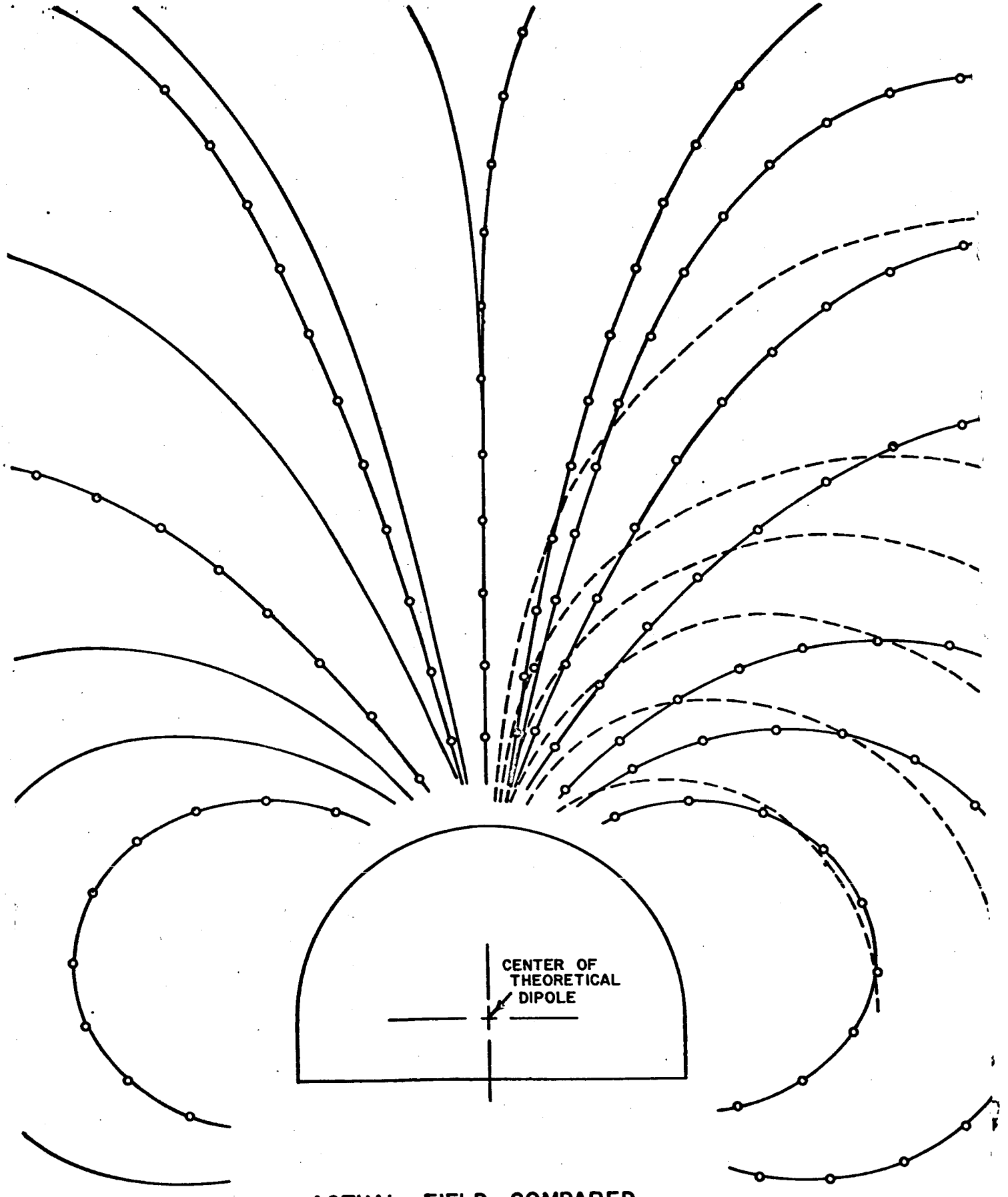

—— ACTUAL FIELD LINES
– – – ANALYTICAL FIELD LINES
o DATA POINTS

ACTUAL FIELD COMPARED TO ANALYTICAL DIPOLE

FIG. 2.1.3

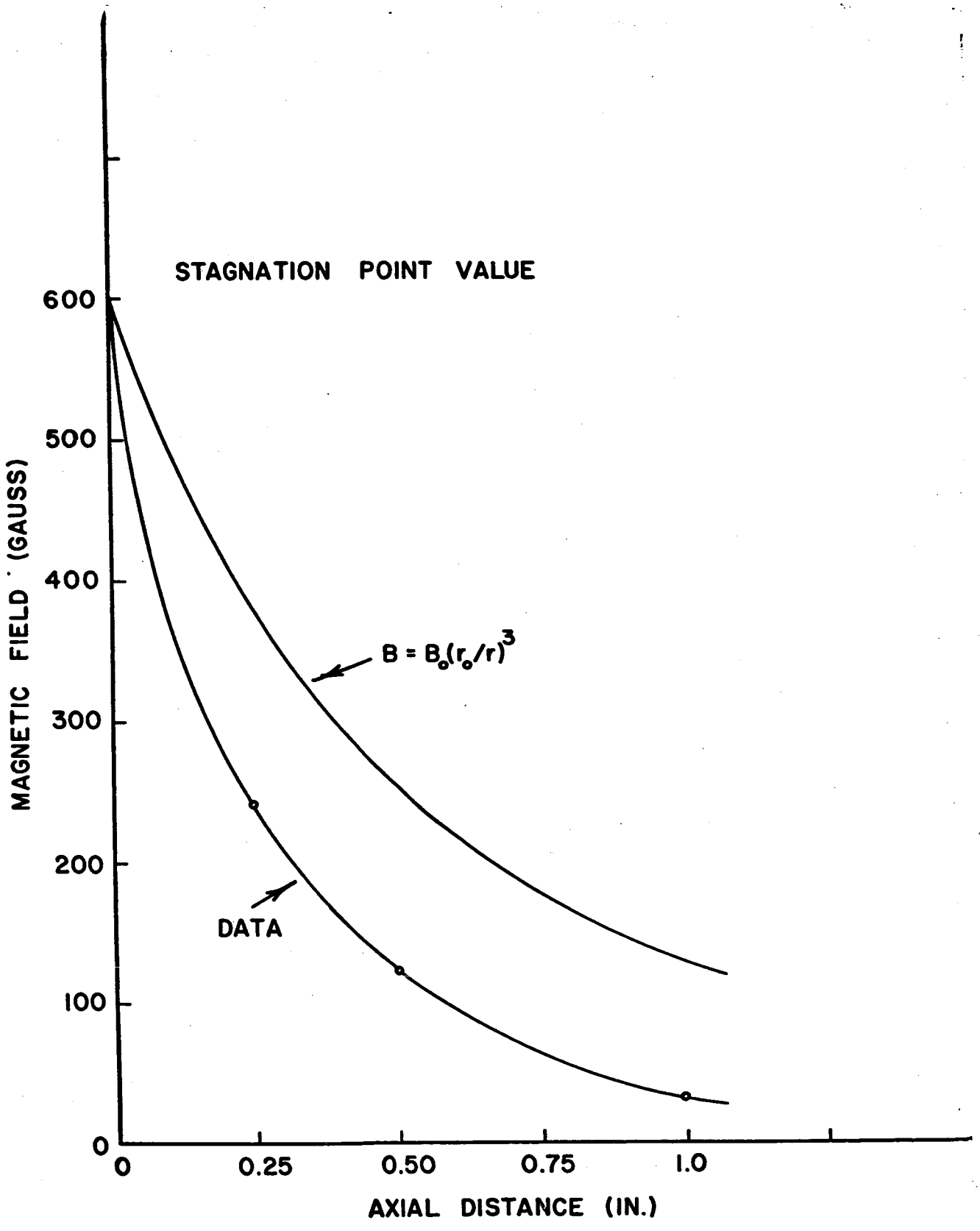

AXIAL FIELD DISTRIBUTION

FIG. 2.1.4

P_{02}/P_1 = STAGNATION PRESSURE RATIO

P_{2w}/P_1 = WEDGE PRESSURE RATIO, 15° WEDGE

FLOW RATE = 0.27 LB ARGON / MIN

INPUT POWER = 30.7 KW

PROBE LOCATION = 8.3 NOZZLE DIAMETERS

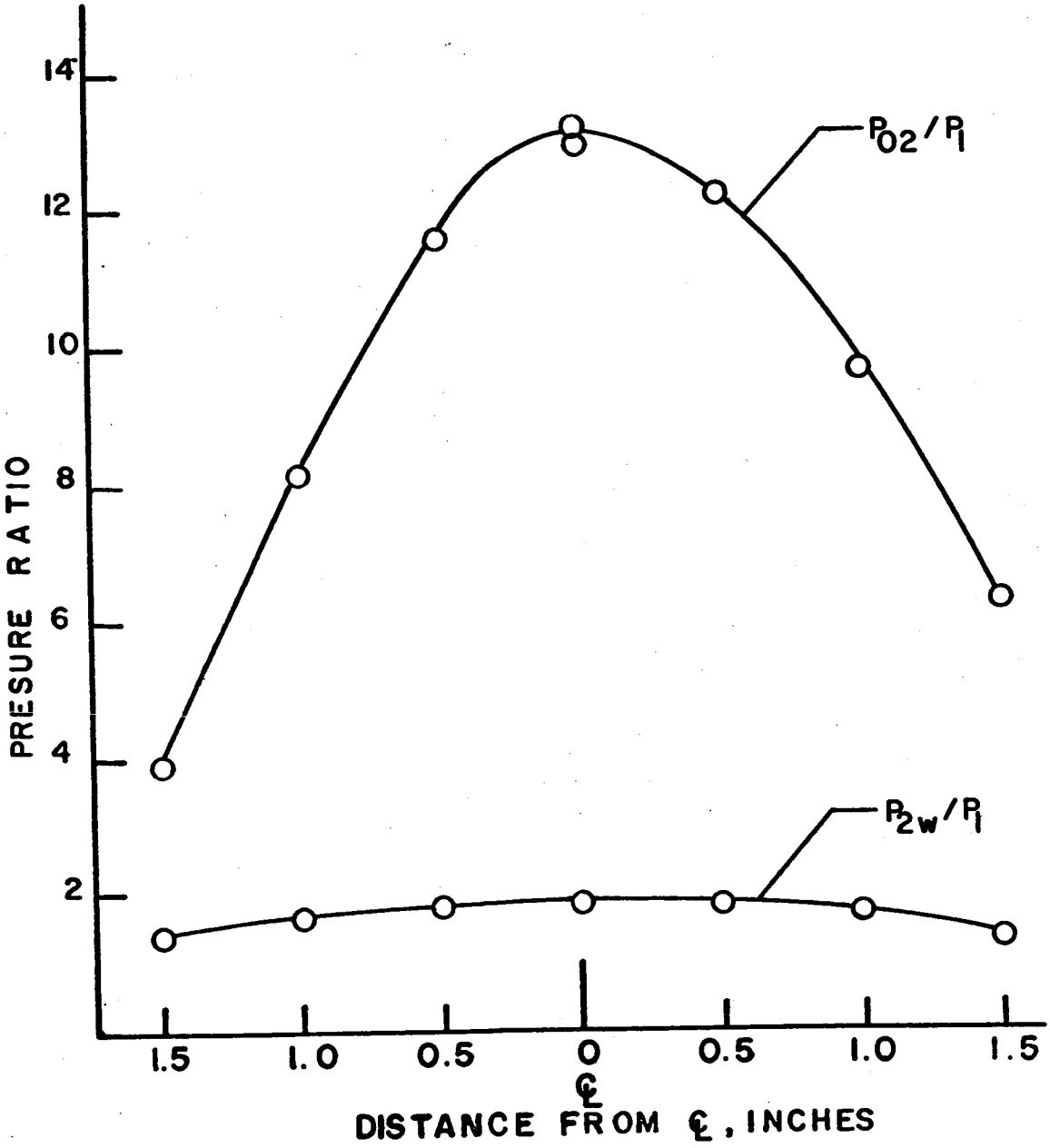

PRESSURE RATIO VRS DISTANCE FROM ℄

FIG. 2.2.1

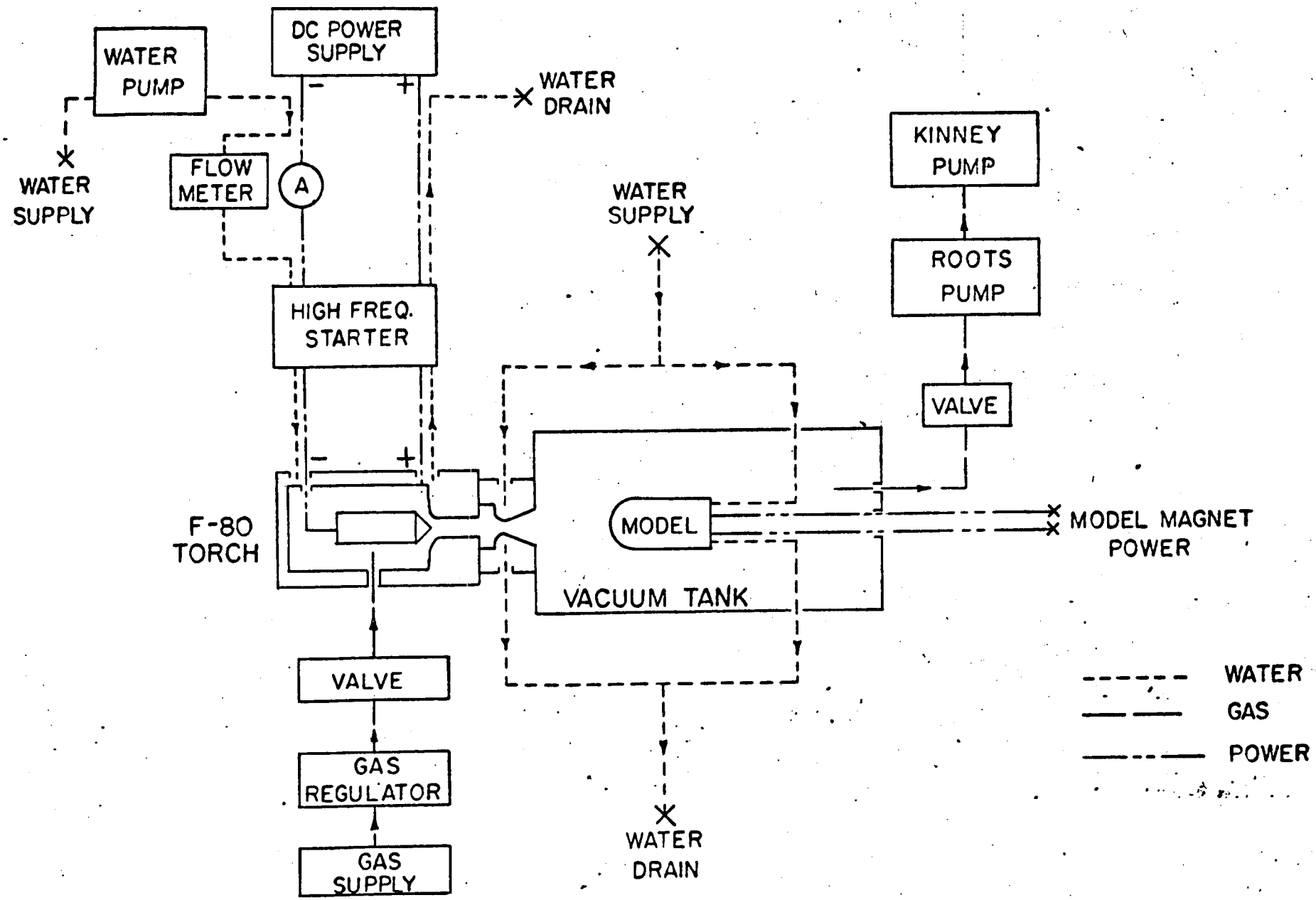

MHD DRAG FACILITY

FIG. 2.3.1

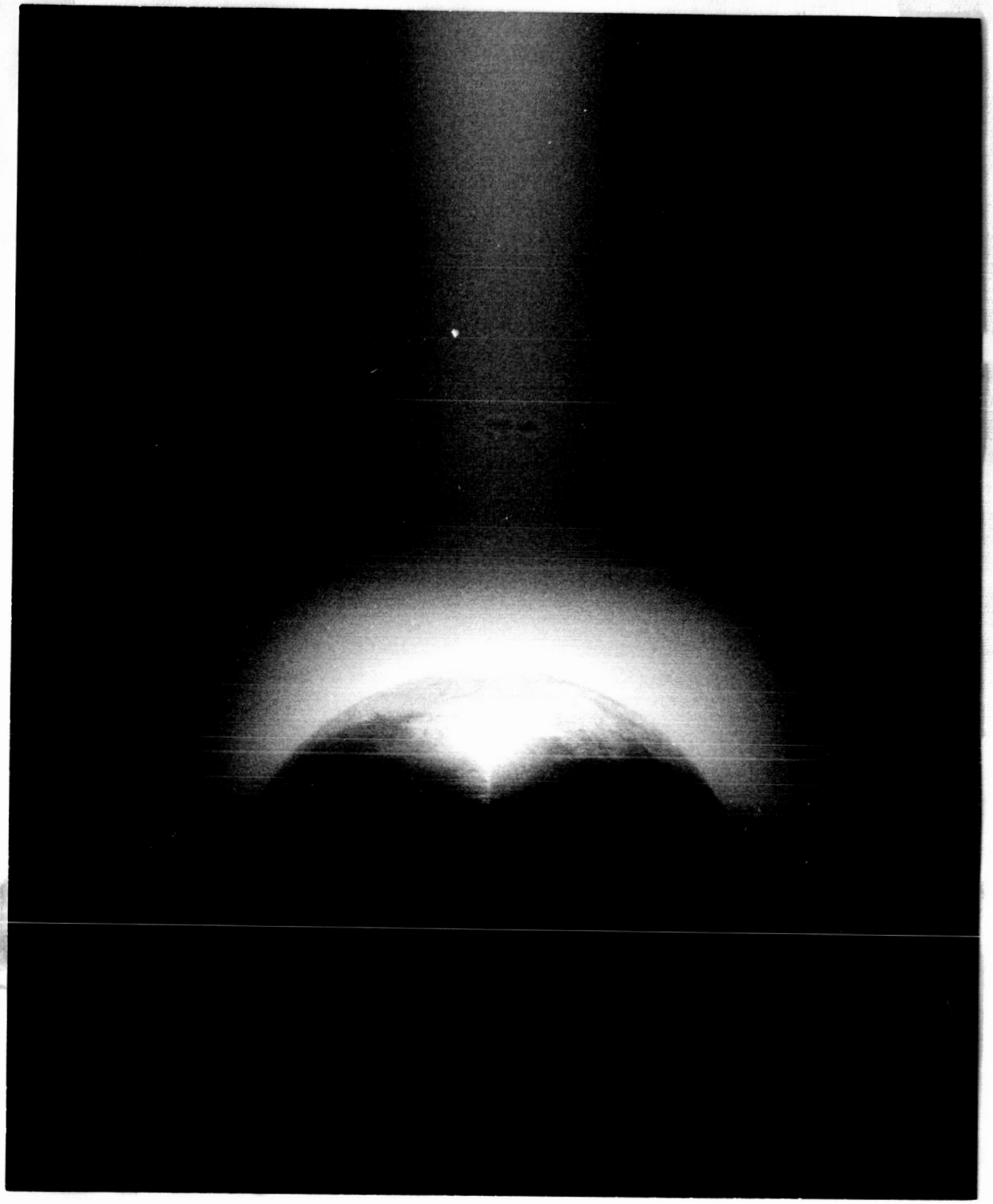

BODY IN FLOW WITHOUT MAGNETIC FIELD

FIG. 2.3.2

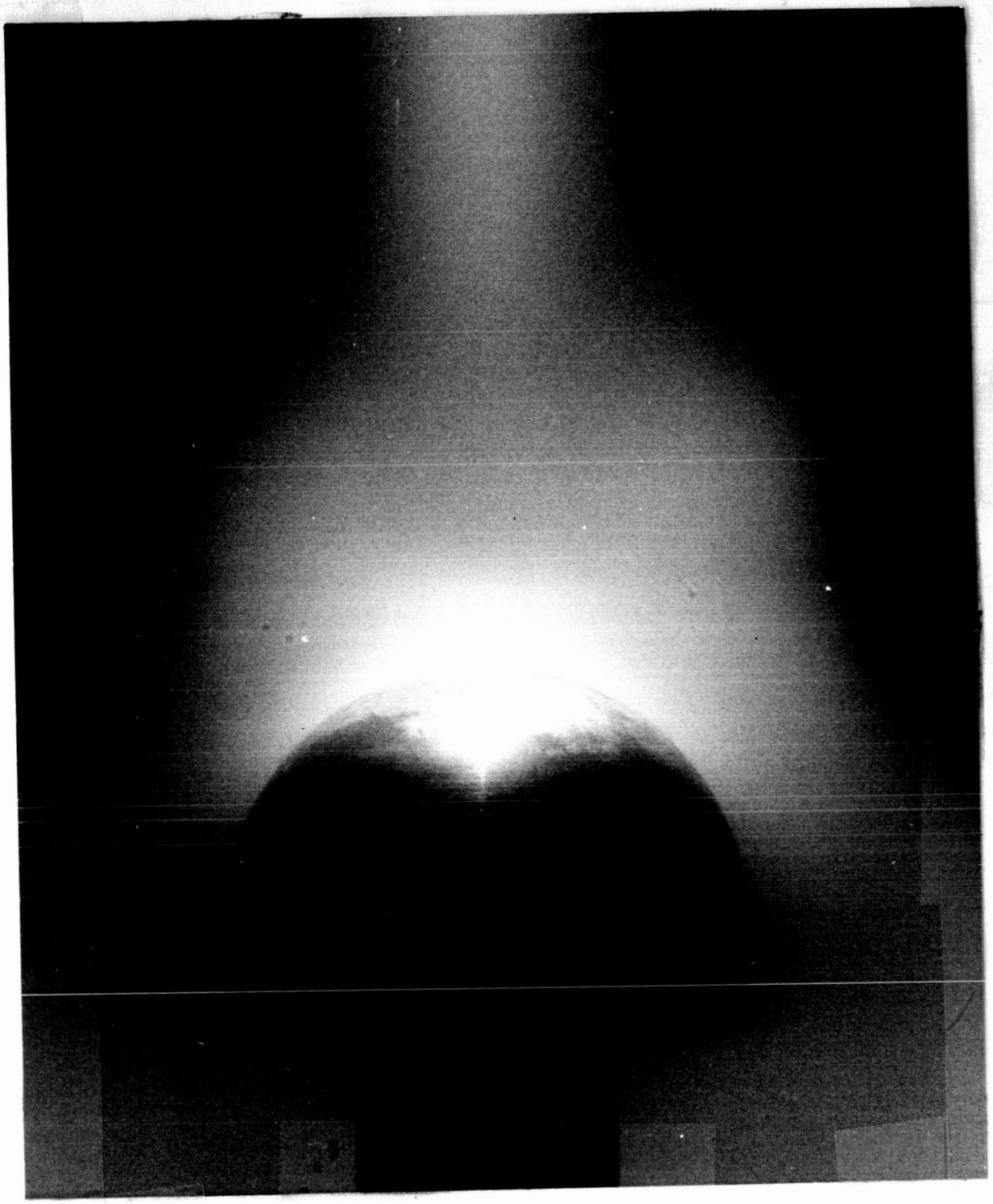

BODY IN FLOW WITH MAGNETIC FIELD

FIG. 2.3.3

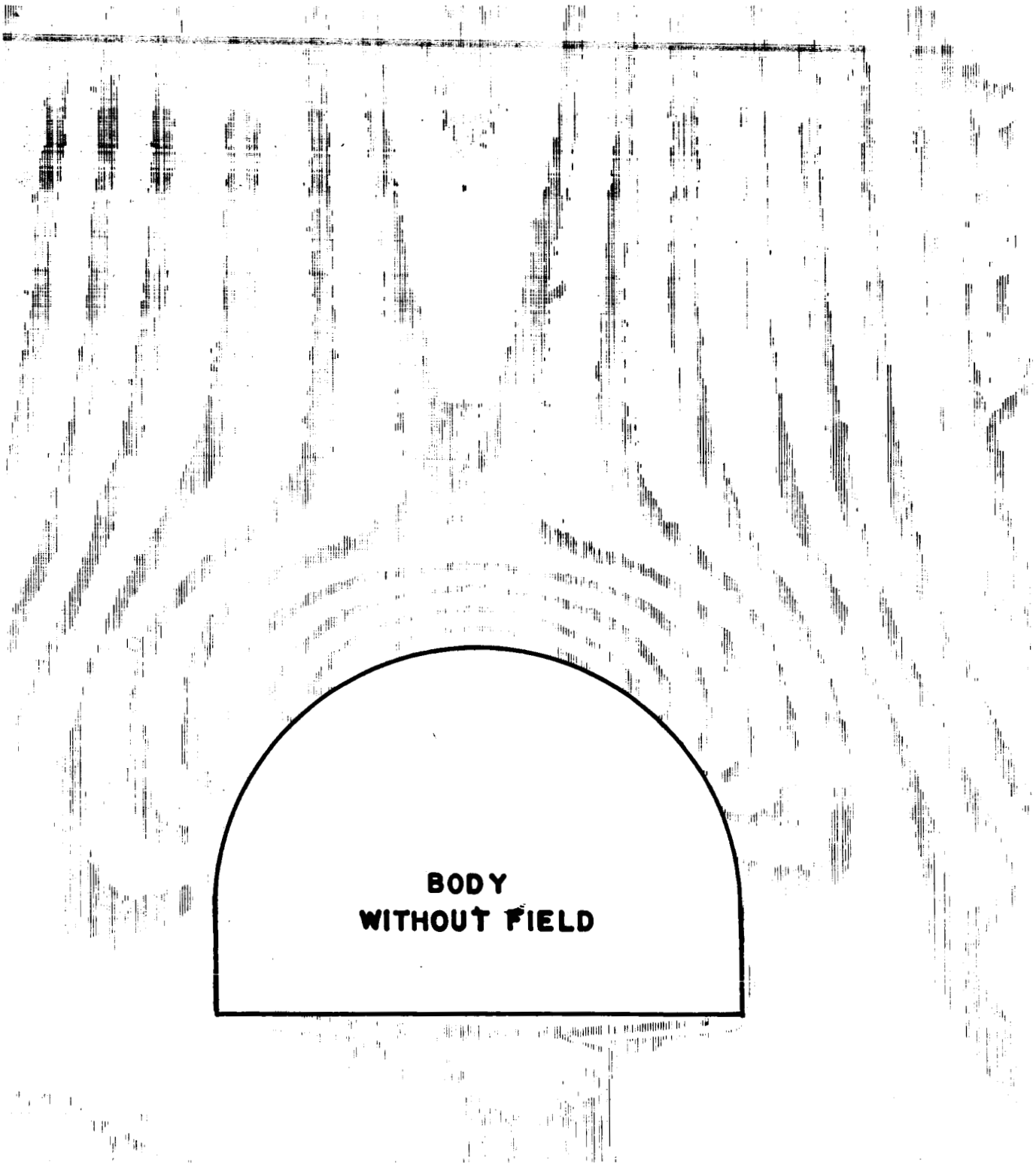

ISO-DENSITY TRACE OF PLASMA NEAR BODY
WITHOUT MAGNETIC FIELD

FIG. 2.3.4

ISO-DENSITY TRACE OF PLASMA
NEAR BODY- WITH MAGNETIC FIELD

FIG. 2.3.5

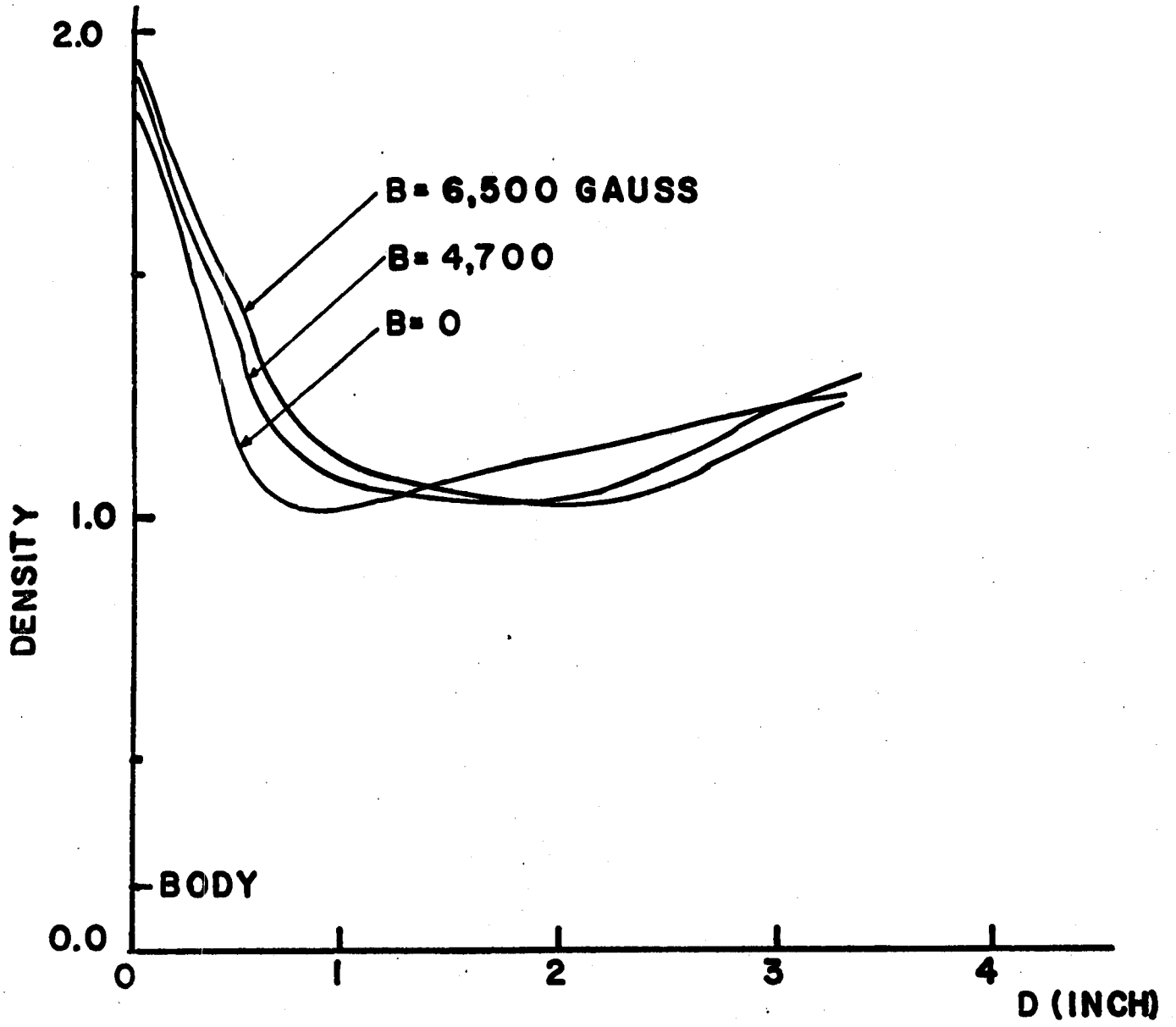

FILM DENSITY VS DISTANCE FROM BODY

FIG. 2.3.6

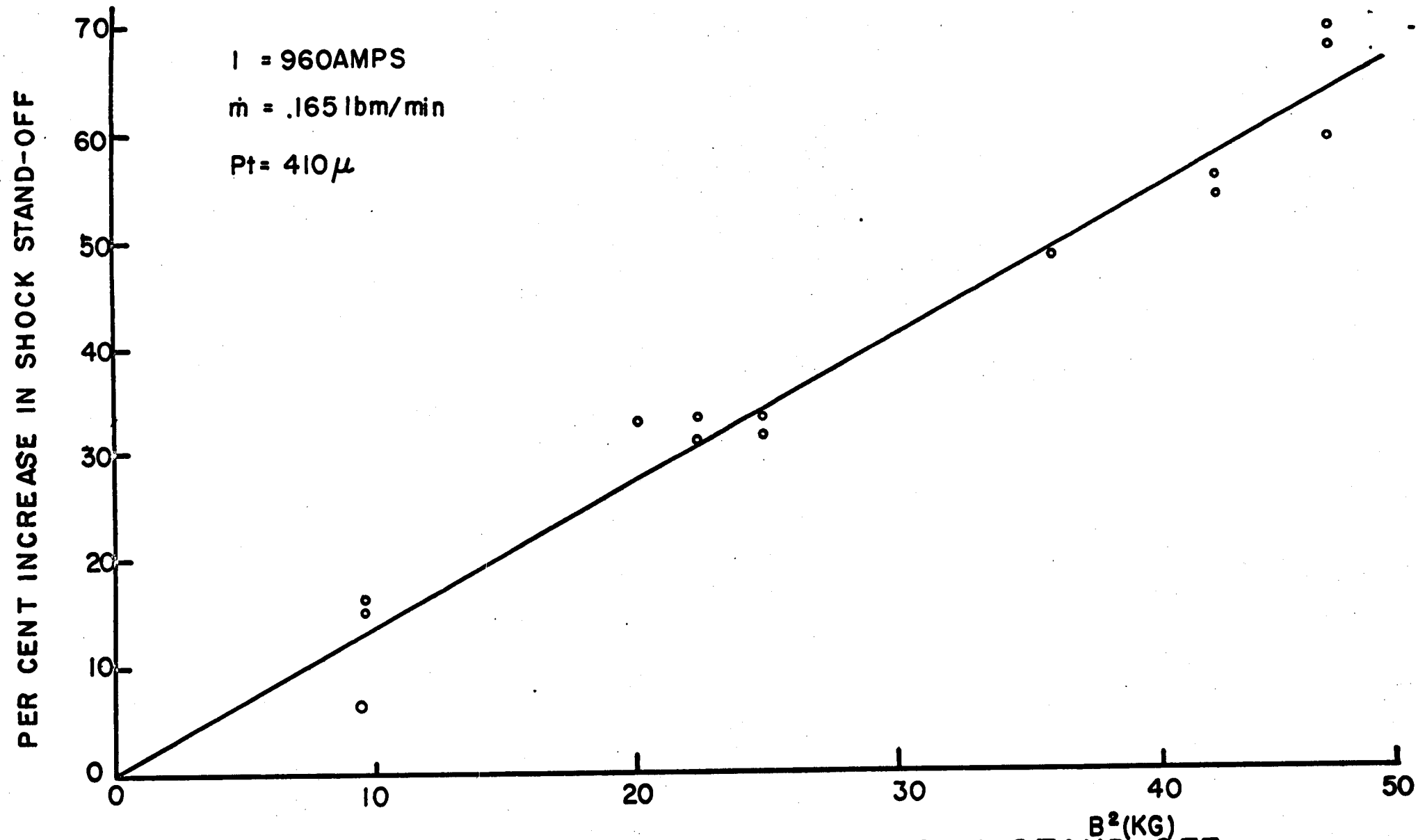

EFFECT OF MAGNETIC FIELD ON SHOCK STAND-OFF DISTANCE

FIG. 23.7

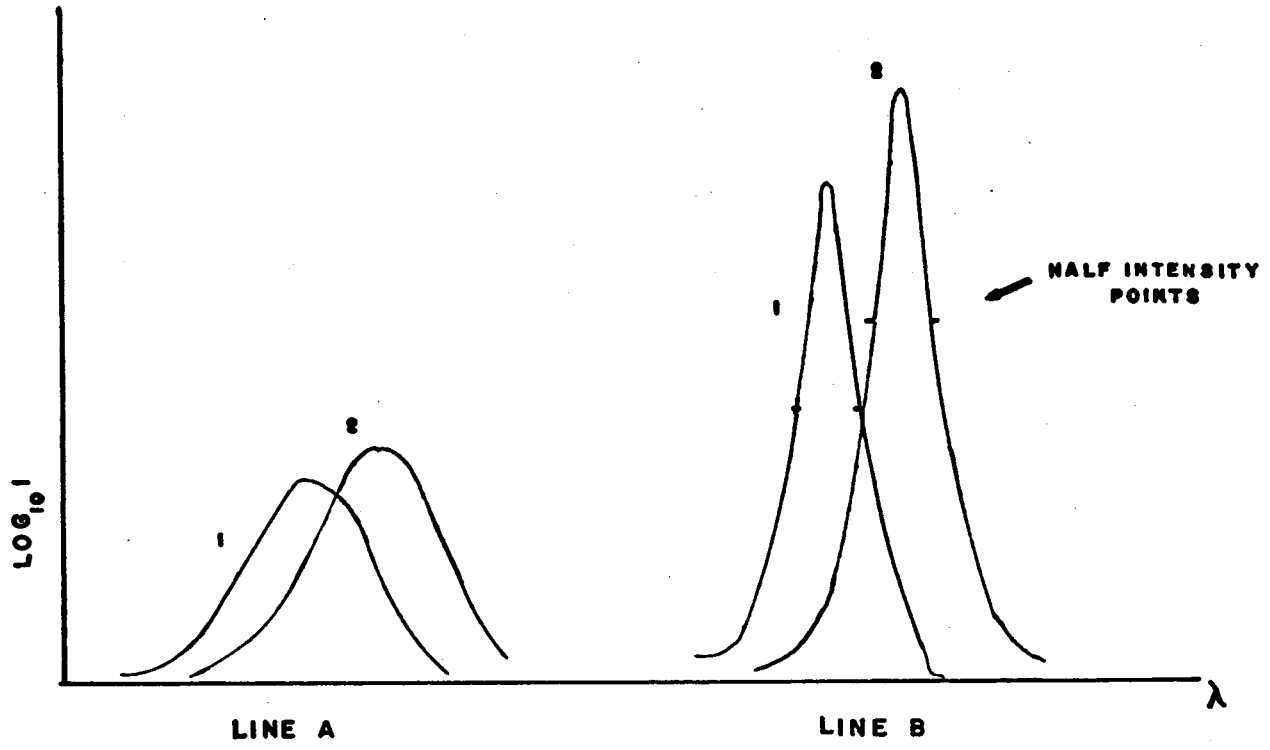

ALTERATION IN INTENSITY WITH MAGNETIC FIELD FOR TWO TYPICAL LINES

1. WITHOUT FIELD
2. WITH FIELD

FIG. 2.3.8

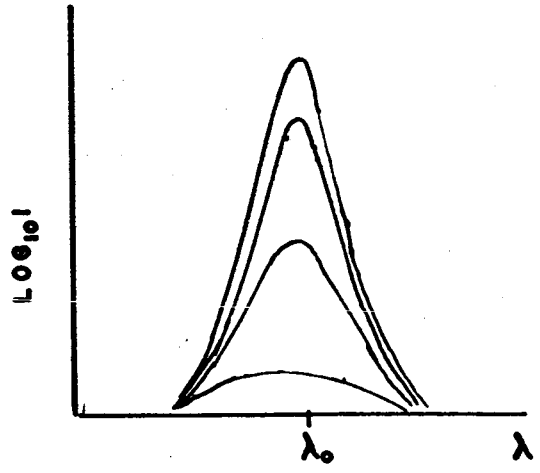

THE DECREASE IN INTENSITY OF A GIVEN LINE ALONG THE AXIAL DIRECTION (NO FIELD)

FIG. 2.3.9

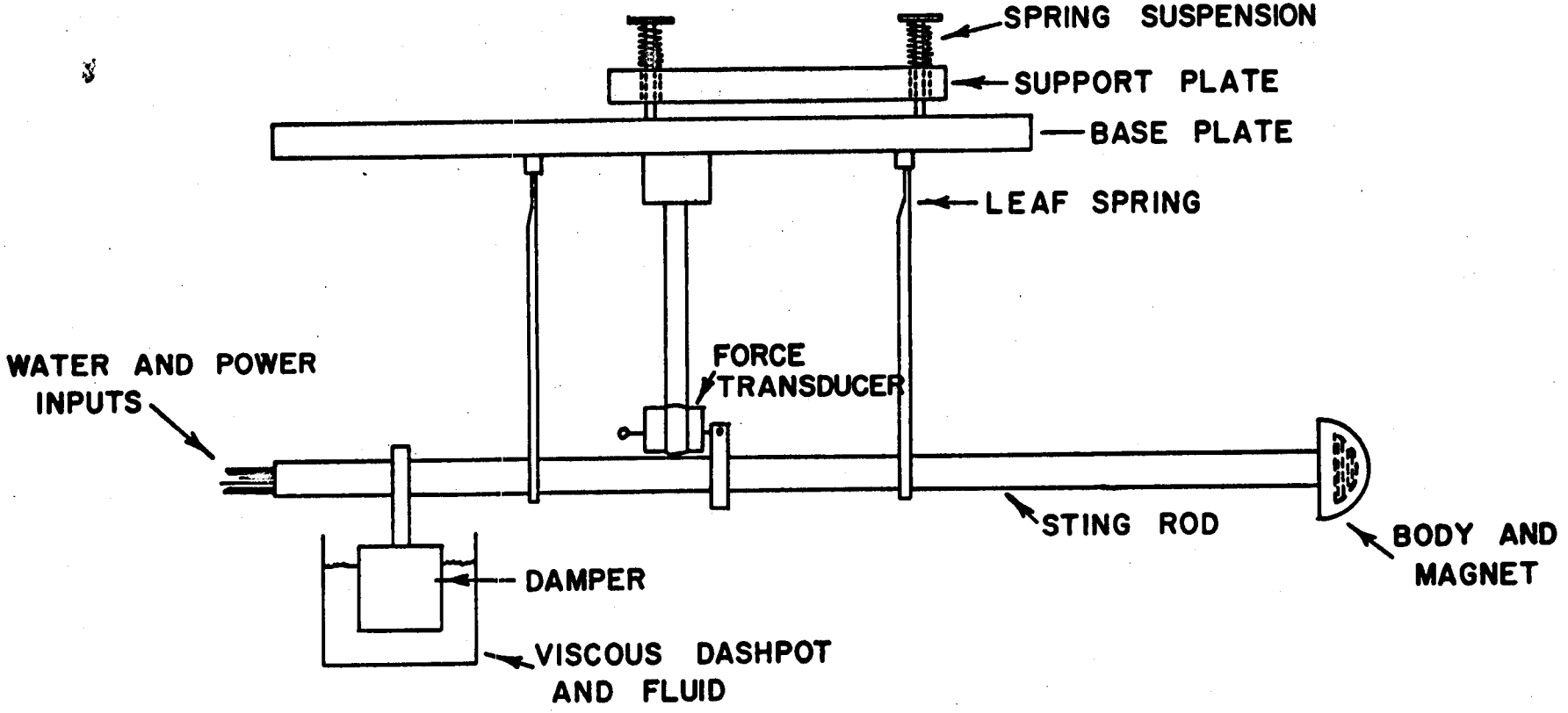

SCHEMATIC OF DRAG MEASUREMENT APPARATUS

FIG. 2.4.1

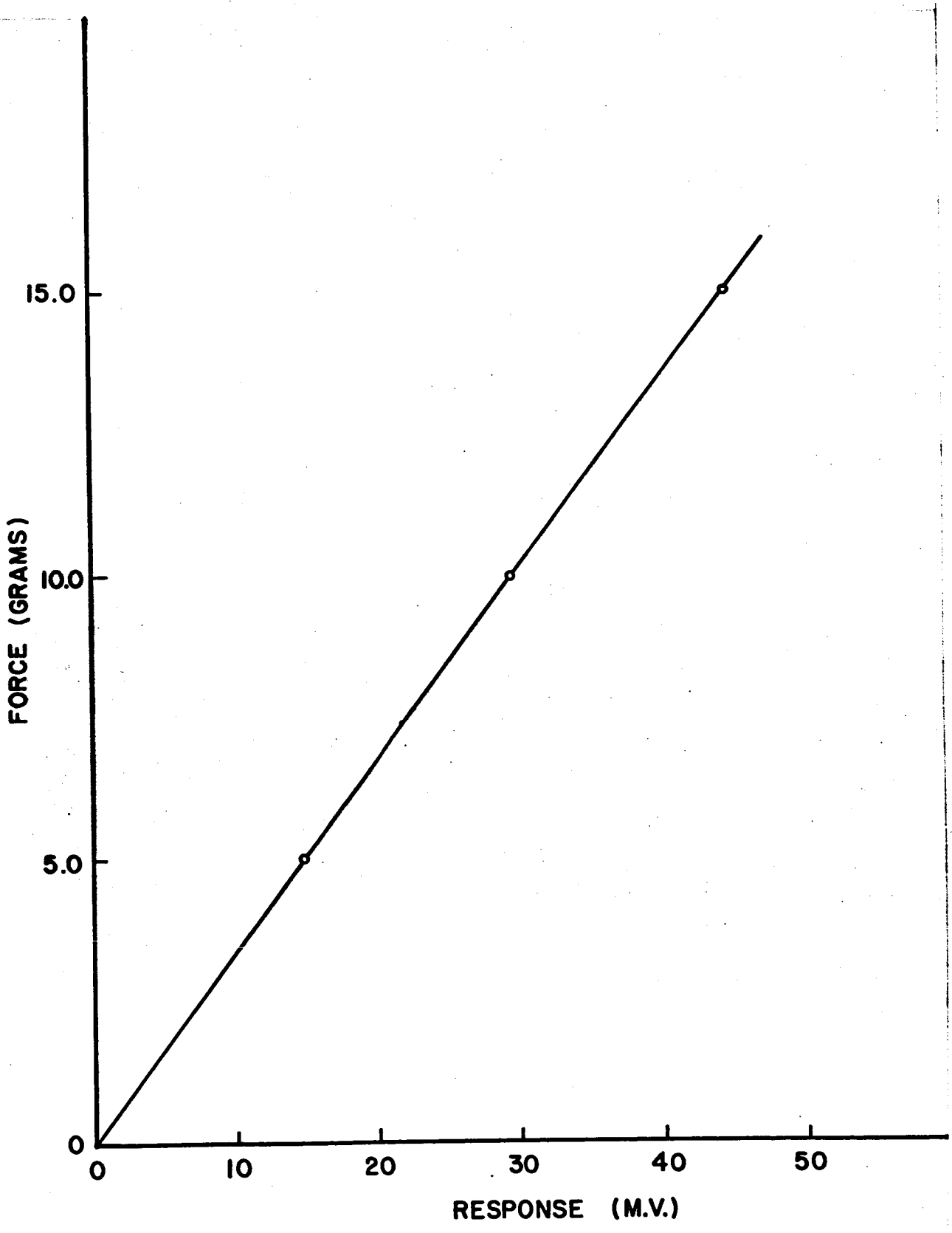

FORCE BALANCE CALIBRATION
(MHD COMPONENT)

FIG. 24.2

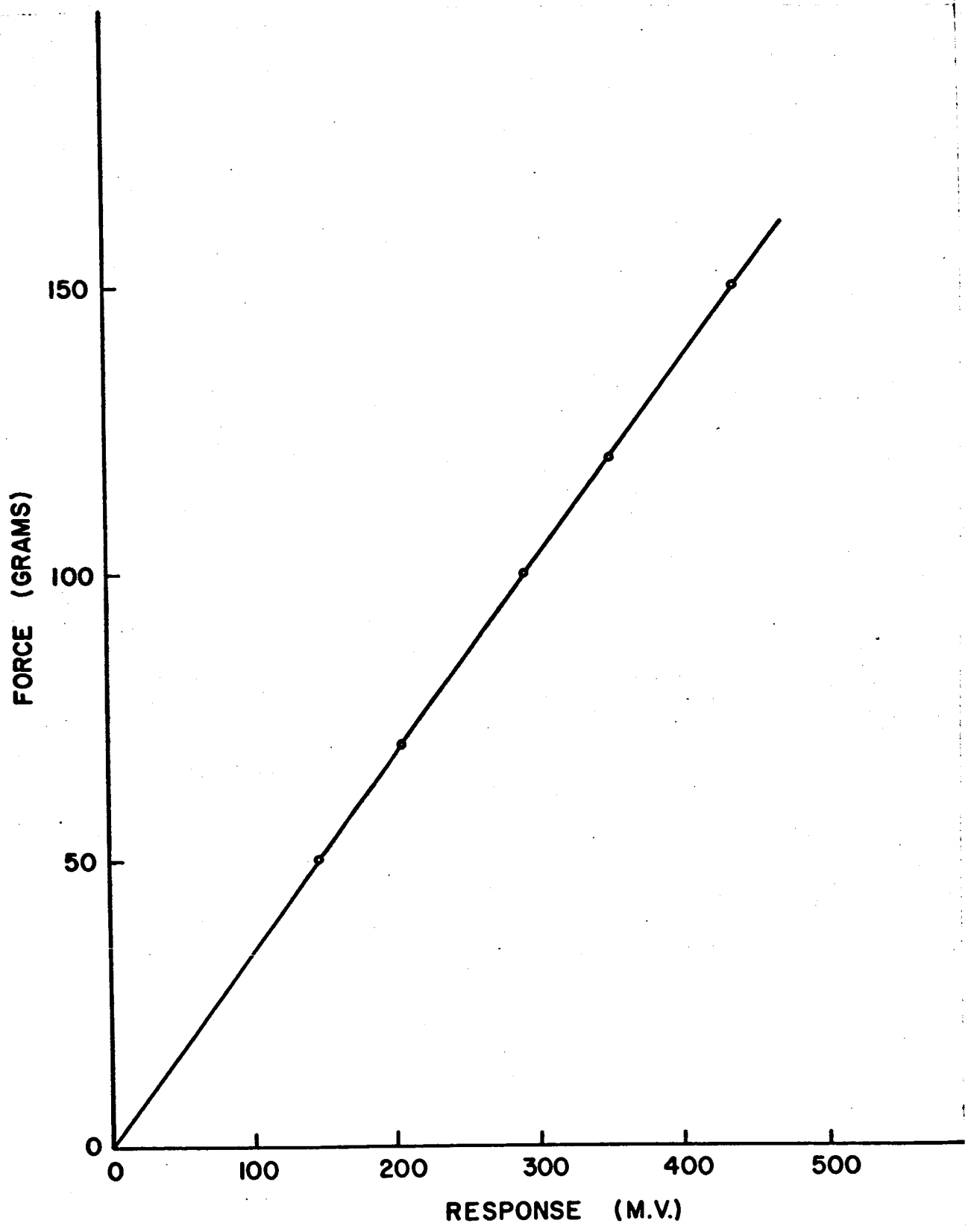

FORCE BALANCE CALIBRATION
(AERODYNAMIC COMPONENT)

FIG. 2.4.3

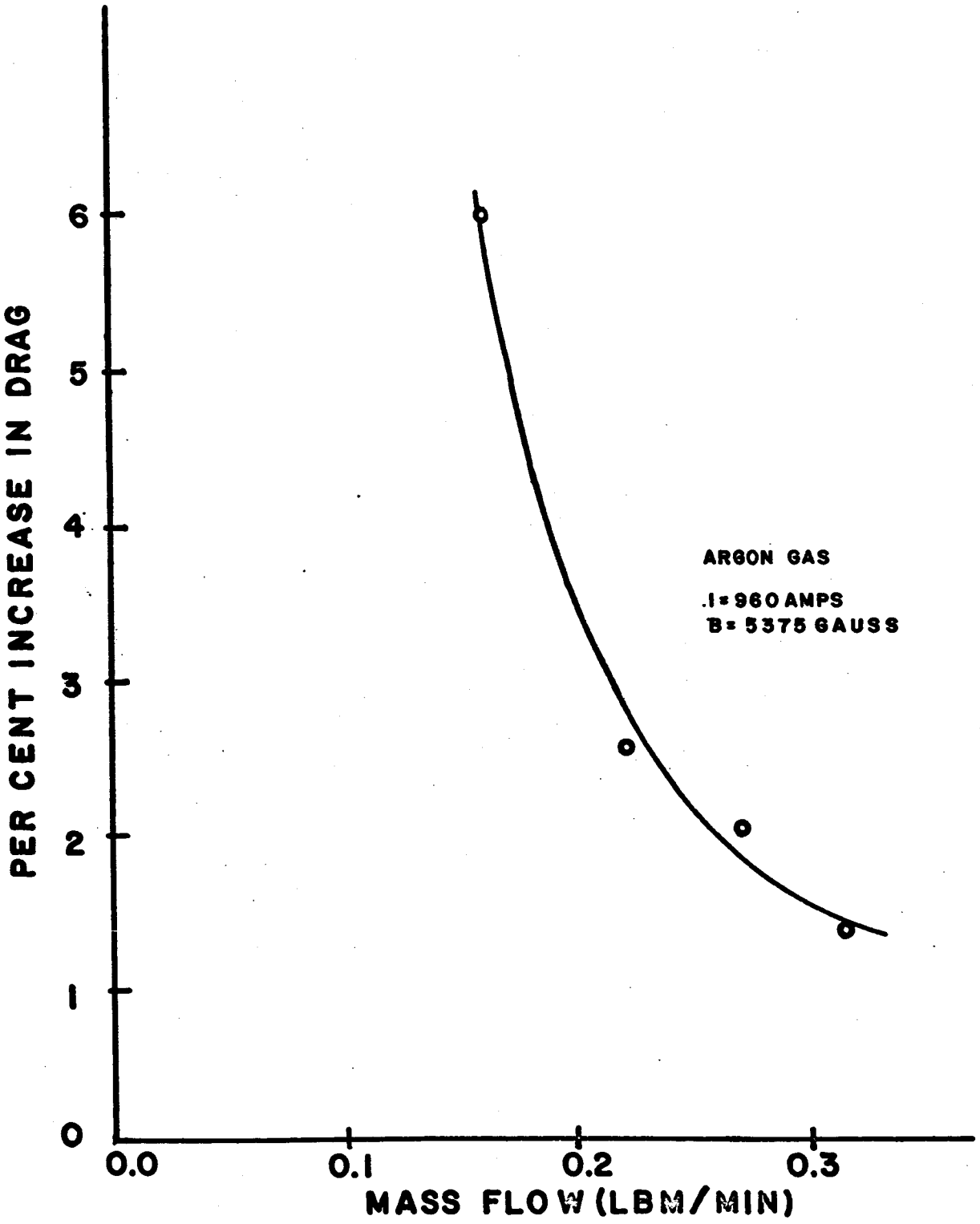

EFFECT OF MASS FLOW AT CONSTANT MAGNETIC FIELD

FIG. 2.4.4

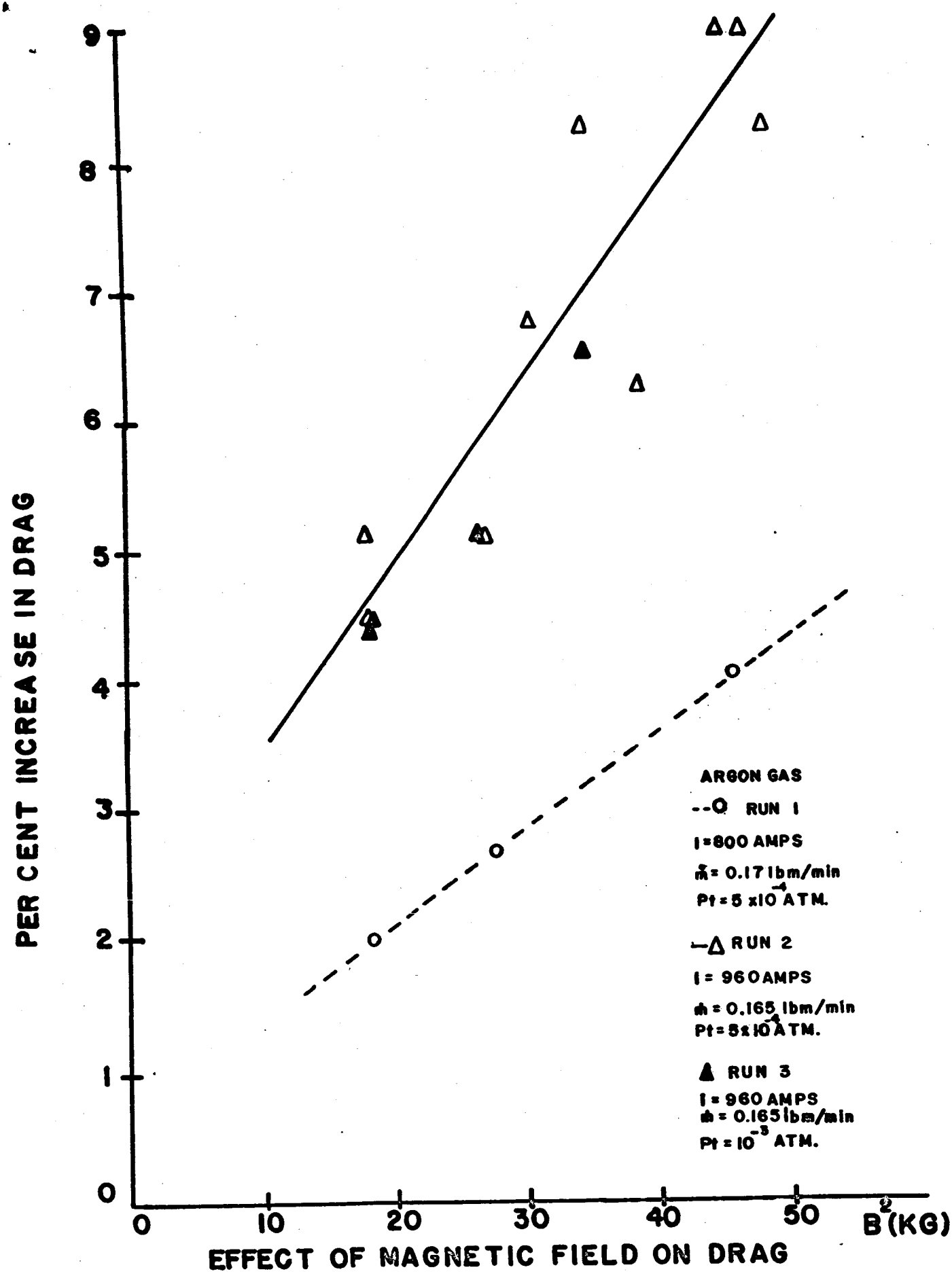
PER CENT INCREASE IN DRAG
0
1
2
3
4
5
6
7
8
9
0
10
20
30
40
50
B² (KG)
EFFECT OF MAGNETIC FIELD ON DRAG
ARGON GAS
--O RUN 1
I = 800 AMPS
ṁ = 0.171 lbm/min
Pt = 5 x 10⁻⁴ ATM.
—Δ RUN 2
I = 960 AMPS
ṁ = 0.165 lbm/min
Pt = 5 x 10⁻⁴ ATM.
▲ RUN 3
I = 960 AMPS
ṁ = 0.165 lbm/min
Pt = 10⁻³ ATM.

FIG. 2.4.5

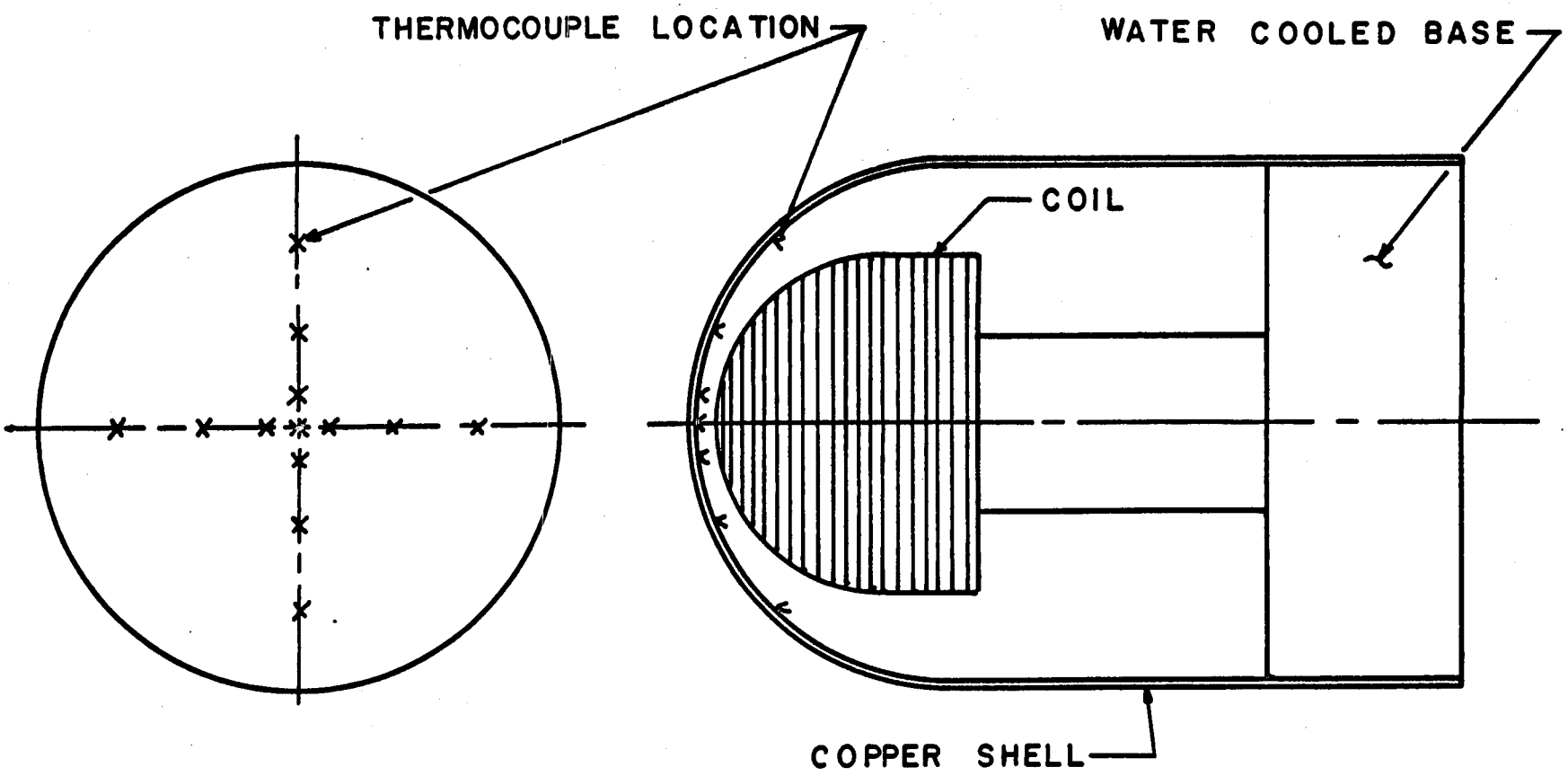

HEAT TRANSFER MODEL

FIG. 2.5.1

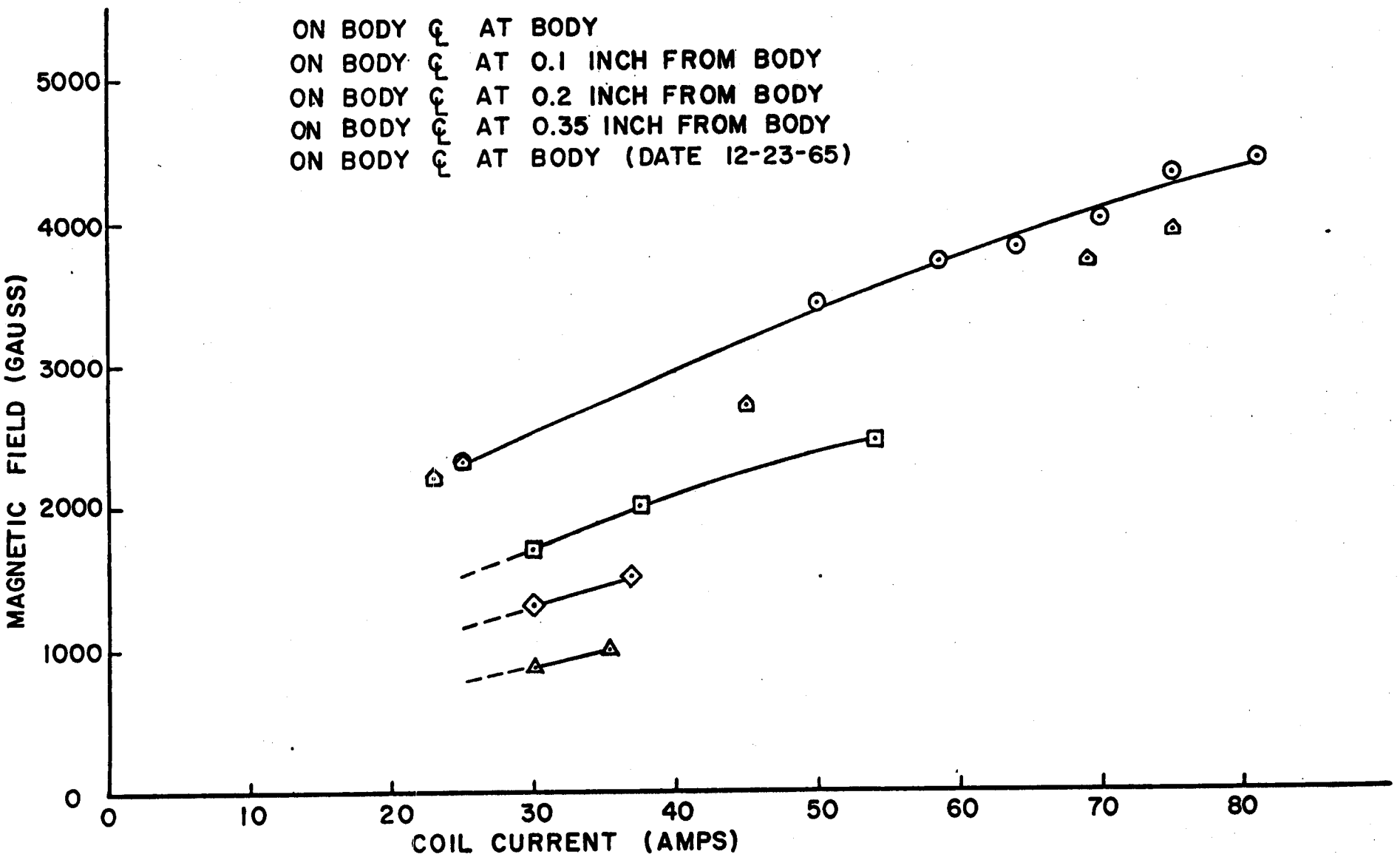

MAGNETIC FIELD VS COIL CURRENT
(FOR HEAT TRANSFER MODEL)

FIG. 2.5.2

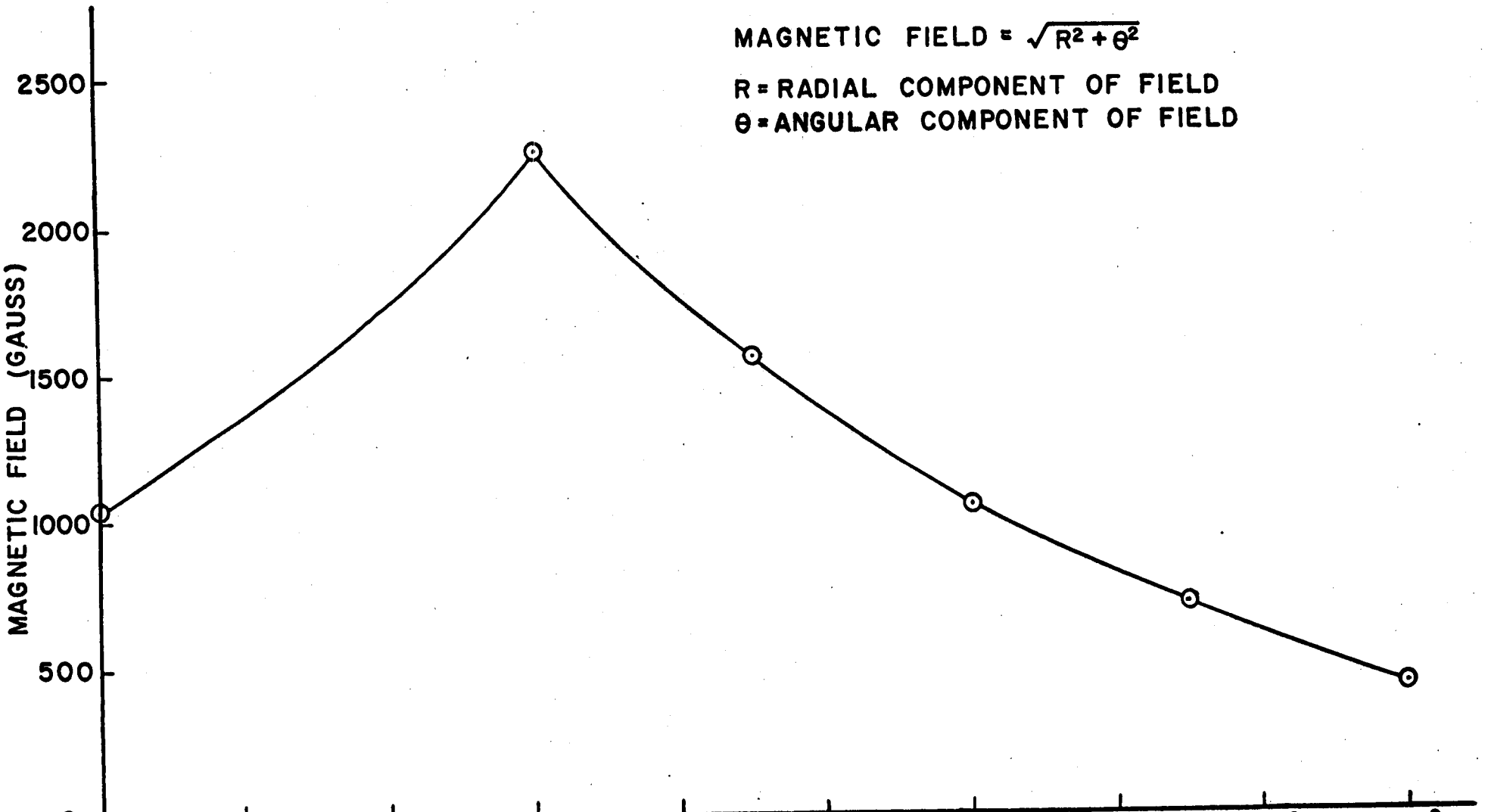

MAGNETIC FIELD OVER SURFACE OF BODY (AT THE BODY)

FIG. 2.5.3